COMPARATIVE STUDY OF THE TRANSMISSION ELLIPSOMETRIC FUNCTION CONTOURS AND THE SMITH CHART

A Thesis
Presented to
The Academic Faculty

By

Wade A. Berzett

In Partial Fulfillment
Of the Requirements for the Degree
Master of Science in Electrical Engineering

Georgia Institute of Technology

August 2006

COMPARATIVE STUDY OF THE TRANSMISSION ELLIPSOMETRIC FUNCTION CONTOURS AND THE SMITH CHART

Approved by:

Dr. A. Rahmen M. Zaghloul, Advisor
School of Electrical and Computer Engineering
Georgia Institute of Technology

Dr. W. Russell Callen
School of Electrical and Computer Engineering
Georgia Institute of Technology

Dr. P. Douglas Yoder
School of Electrical and Computer Engineering
Georgia Institute of Technology

Date Approved: 10 July 2006

Much education today is monumentally ineffective.

All too often

we are giving young people cut flowers

when we should be teaching them

to grow their own plants.

John W. Gardner

ACKNOWLEDGEMENTS

I would like to extend a debt of gratitude to David A. Keeling for all of his help and support. I would like to thank my advisor, Dr. A. Rahmen Zaghloul for not giving me ‘cut flowers’. And finally, I want to thank my reading committee for their valuable critique.

TABLE OF CONTENTS

LIST OF FIGURES

SUMMARY

Transmission ellipsometry is governed by the transmission ellipsometric function (TEF) of a film-substrate system. The function can be analyzed through a series of constant-thickness contours and constant-angle-of-incidence contours in the complex plane. It has been observed that these TEF contours for a zero film-substrate system bear strong resemblances to the families of curves that make up the Smith chart for transmission lines.

In this thesis we present a comparative study of the TEF and the Smith chart, specifically through the distinct similarities of their respective families of curves. It is shown that both TEF and Smith chart have similar contours in both the positive and negative imaginary half planes. The Smith chart's contours originate from a complex plane with linear boundaries. It is bisected into symmetric positive and negative imaginary half planes of equal areas that are conjugate of each other. When transformed to the Smith chart, it is normalized and the conjugate relationship remains intact. All contours in the positive imaginary half plane of the Smith chart are symmetric to all of the contours in the negative half plane of the Smith chart. TEF contours originate from a non-complex reduced thickness plane. This plane has a non-linear upper boundary. It is bisected into two equal areas but non-symmetric, half planes. When transformed to the complex τ plane, the likeness of the constant-angle-of-incidence contours and constant-thickness contours to the Smith chart contours become a function of the material indices. As the film-substrate systems material indices are increased, the range of the non-linear boundary of the $\phi_0 - d_r$ plane is reduced and the TEF contours more closely resemble the Smith chart.

CHAPTER I
INTRODUCTION

The transmission ellipsometric function τ (TEF), governs the change in polarization of an electromagnetic wave incident on, and transmitted through a film substrate system. [1-3] Its derivation, like the ellipsometric function for reflection, ρ, is the Drude equation. [4, 5] The TEF is used in industry for the analysis and design of various transparent coatings and applications. The following are a few examples.

Ellipsometric memory was first introduced in 1994 using reflection ellipsometry (ρ). [6, 7] Though innovative, it was determined to be difficult to implement due to large memory cell sizes required for higher angles of incidence. This downside was overcome in reference [8] by using transmission ellipsometry (τ) for a transparent type ellipsometric memory. By capitalizing on the normal incidence angle, they were able to significantly reduce required cell sizes. They were able to devise a 4-bit transparent memory cell through model calculations and a 2-bit cell through preliminary experiments.

A linear partial polarizer (LPP) is a device that allows zero relative phase shift between the transmitted and incident wave components parallel, *p*, and perpendicular, *s*, to the plane of incidence with relative amplitude attenuation. Reference [9] shows how the TEF transforms ordered pairs (ϕ_0, d_r) of a negative* film-substrate system, angle of incidence and film thickness respectively, into polar curves on the τ plane. This illustrative representation of a film-substrate system in the τ plane allows for a simple qualification when the system behaves as an LPP with highly accurate results. Reference [1] revealed

* Negative film-substrate systems will be defined and discussed in section 4.2.1.

that by analyzing the TEF through its constant angle of incidence contours (τCAICs) and constant thickness contours (τCTCs), zero[†] film-substrate device designs are possible that simultaneously behave as an LPP and induce zero relative change in polarization between the transmitted and incident wave.

The Smith chart, first introduced in 1939, [10] is a highly versatile and well distributed method for solving problems involving electromagnetic wave propagation. [11] Its graphical representation of complex impedance has been used in a multitude of applications, making complex calculations easier, and with relatively high accuracy. Though initially created to aid in solving transmission line problems, the Smith chart has been found to be useful in many arenas of study. The following are a few examples.

By superimposing the power output curves of magnetron or klystron tubes onto a Smith chart, the Smith chart is used to develop the Rieke chart. [12] It is used to help find stable power ranges for magnetrons and klystrons under variable microwave impedance conditions. The Rieke chart is also used to estimate the effect of reflections from the window on a gyrotron.

It is recognized that the complex analysis for the frequency response of pneumatic transmission line systems is similar to that of the Smith chart theory. [13] By modeling the Smith chart and using reflection coefficients and mapping, it proposed a graphical method to calculate the frequency response of a pneumatic transmission line system. This innovative method provides significant insight for analyzing and designing pneumatic systems. [13]

The Smith chart has also been found to be useful in the field of quantum mechanics. [14] It has been found that the impedance matching of the Smith chart amounts to the

[†] Zero film-substrate systems will be defined and discussed in section 4.2.2.

extraction of the complex reflection coefficient from the wave function. This coefficient can be directly used to derive an elementary Wentzel-Kramers-Brillouin (WKB) quantization condition. [14]

Even with the advent of the computer the analog Smith chart's usefulness continues as its fundamental theory and visual graphics are programmed into various software modeling tools, thus allowing a greater range of versatility and use. [15-18]

Distinct similarities have been found to exist between transmission ellipsometric function contours of a film-substrate system and Smith chart contours of transmission lines. The comparison of these two systems of contours may enlighten future efforts in developing innovative tools, similar to that of the Smith chart, for optical transmission applications.

This thesis is organized into five chapters. Chapter 1 provides an introduction to the transmission ellipsometric function and Smith chart. Examples of their use and applications are presented following each respective introduction. Chapter 2 defines and provides previous research on the transmission ellipsometric function. Chapter 3 explains what the Smith chart is and how it is composed. Chapter 4 presents a comparative analysis of the τ plane constant-thickness contours and constant-angle-of-incidence contours with the respective contours of the Smith chart. It also presents a description of the transmission ellipsometric function contours for material composition of indices significantly larger that those currently being used. Finally, Chapter 5 provides conclusions to the research presented.

CHAPTER II
TRANSMISSION ELLIPSOMETRIC FUNCTION

2.1 INTRODUCTION

The transmission ellipsometric function (TEF) τ of a film-substrate system is a mathematical representation of the behavior of the electromagnetic wave upon transmission through a film-substrate system. It is a function of the wavelength of the electromagnetic wave (λ), angle of incidence (ϕ_0), film thickness (d), and the refractive index for the ambient (N_0), film (N_1), and substrate (N_2). It relates the change in polarization of an electromagnetic wave incident upon, and transmitted through, a film substrate system, figure 1. [1, 4, 5]

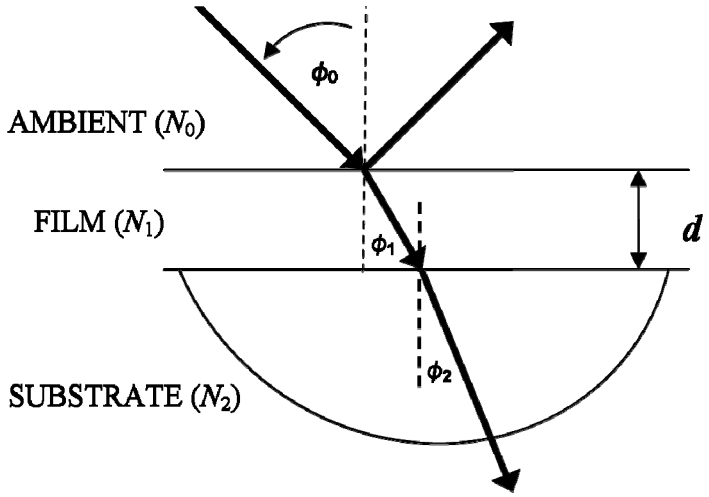

Figure 2.1: Film-substrate system. An electromagnetic wave transmitted through the ambient-film (0-1) and film-substrate (1-2) interface at ϕ_0 and ϕ_1 respectively. To avoid complications arising from reflections and losses at the substrate bottom, the hemispherical surface is assumed to be antireflection coated. [19]

The refractive indices of N_0, N_1, and N_2 are related to the angle of incidence in the ambient

ϕ_0, the angle of refraction into the film ϕ_1, and the angle of refraction into the substrate ϕ_2, by Snell's law which is $N_0 \sin \phi_0 = N_1 \sin \phi_1 = N_2 \sin \phi_2$. The TEF is written as the ratio of the complex amplitude transmission coefficients

$$\tau = \frac{T_p}{T_S}, \tag{1}$$

where

$$\tau = \frac{t_{01p} t_{12p} e^{-j\beta}}{1 + r_{01p} r_{12p} e^{-j2\beta}} \cdot \frac{1 + r_{01s} r_{12s} e^{-j2\beta}}{t_{01s} t_{12s} e^{-j\beta}}. \tag{2}$$

p and *s* are the electric wave vector components parallel (*p*) and perpendicular (*s*) to the plane of incidence. The Fresnel coefficients for transmission are t_{01p}, t_{12p}, t_{01s}, t_{12s} and the Fresnel coefficients for reflection are r_{01p}, r_{12p}, r_{01s}, and r_{12s}. Through direct substitution into Eq. (1) we get

$$\tau = a \cdot \frac{1 + bX}{1 + cX}, \tag{3}$$

where

$$a = \frac{t_{01p} \cdot t_{12p}}{t_{01s} \cdot t_{12s}}, \tag{4}$$

and

$$(b, c) = (r_{01s} \cdot r_{12s}, r_{01p} \cdot r_{12p}). \tag{5}$$

The complex exponential film thickness function is

$$X = e^{-j\frac{4\pi d}{\lambda}\sqrt{N_1^2 - N_0^2 \sin^2 \phi_0}}. \tag{6}$$

Equation (3) shows that TEF is related to *X* by a bilinear transformation, where

$$b \neq c. \tag{7}$$

TEF is also written in the form

$$\tau = \tan\psi e^{j\Delta} \tag{8}$$

where $\tan\psi$ is the p-to-s relative amplitude attenuation and Δ is the p-to-s relative phase shift upon transmission. Both of these angles, ψ and Δ, are measured experimentally.

The general behavior of TEF is determined by the film-substrate system classification. [20, 21] Assuming a three phase system, a film-substrate system is classified into three categories; negative, zero, and positive. The system is negative if $N_1 < \sqrt{N_0 \cdot N_2}$, zero if $N_1 = \sqrt{N_0 \cdot N_2}$, and positive if $N_1 > \sqrt{N_0 \cdot N_2}$.

2.2 ANGLE OF INCIDENCE-FILM THICKNESS PLANE (ϕ_0 – d plane)

Of the variables (N_0, N_1, N_2, λ, ϕ_0, d) used in the calculation of the transmission ellipsometric function, TEF, two are independent of the system's material composition for any wavelength λ; angle of incidence ϕ_0, and film thickness d. These two independent variables, (ϕ_0, d), when plotted against each other, make up the set of all ordered pairs for a film-substrate system; the $\phi_0 - d$ plane. This plane spans $\{[0° \; 90°], [0, \infty \; nm)\}$, respectively. The film thickness period, $D_{\phi 0}$ is given by [1, 22]

$$D_{\phi} = \frac{\lambda}{2\sqrt{N_1^2 - N_0^2 \sin^2 \phi_0}}. \tag{9}$$

It is a periodic function of the film thickness d and repeats itself every $mD_{\phi 0}$ where m=1,2,3… . It has been previously shown in reference [22] that multiple periods of $mD_{\phi 0}$, figure 2.2, can be reduced to a single period of $D_{\phi 0}$ and represented by the reduced

thickness plane, $\phi_0 - d_r$ plane, whose new limits are $0 \leq \phi_0 \leq 90°$ and $0 \leq d \leq D_{\phi_0}$, figure 2.3.

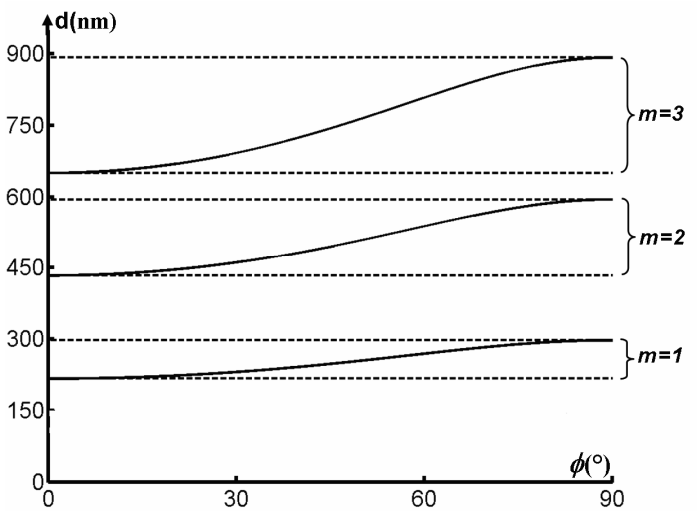

Figure 2.2: The $\phi_0 - d$ plane where $N_0 = 1.0$ and $N_1 = 1.46$ at $\lambda = 632.8$ nm, illustrating mD_{ϕ_0} curves at multiples of 1, 2, and 3.

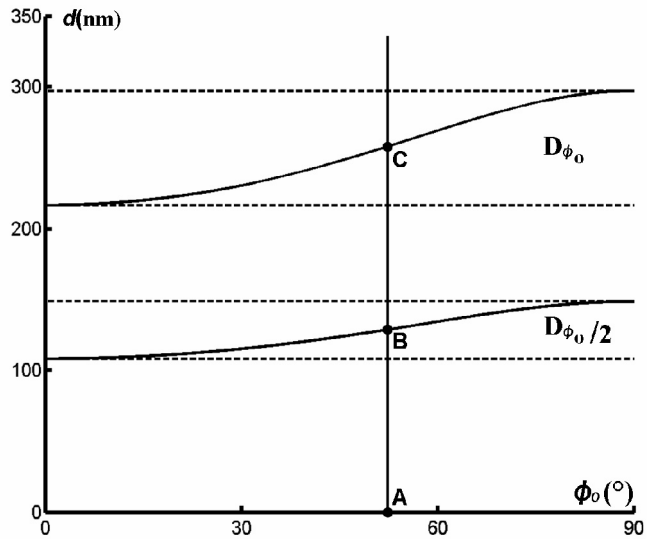

Figure 2.3: The $\phi_0 - d_r$ plane where $N_0 = 1.0$ and $N_1 = 1.46$ at λ=632.8 nm. The points A, B, and C represent a film thicknesses of 0 nm (bare substrate), $D_{\phi_0}/2$, and D_{ϕ_0}, respectively.

2.3 COMPLEX EXPONENTIAL FILM THICKNESS PLANE (X PLANE)

The complex exponential film thickness function X transforms the $\phi_0 - d_r$ plane to the intermediate complex exponential film thickness plane, the X plane. Given a transparent film, $|X| = 1$ for any angle of incidence or film thickness and Eq. (6) can be thereby represented by a circle or arc on the X plane unit circle. [22] Every point on the $\phi_0 - d_r$ plane can be successively transformed onto the τ plane through this X plane, by the TEF. [1]

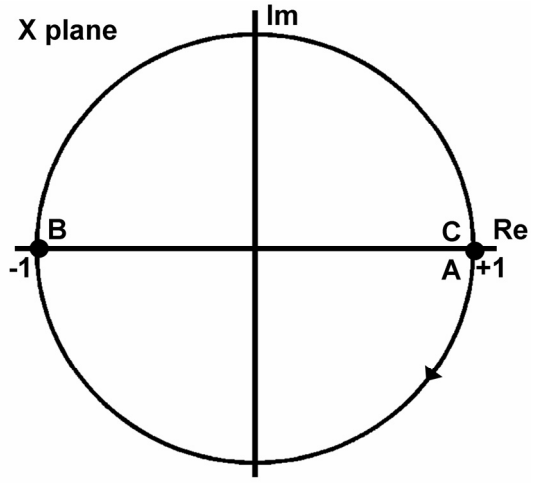

Figure 2.4: The X plane. The points A, B, and C correspond to ordered pairs on the $\phi_0 - d_r$ plane from figure 2.3.

2.3.1 X Plane Constant-Angle-of-Incidence Contours (XCAICs)

From figure 2.3, vertical lines on the $\phi_0 - d_r$ plane, drawn normal to the ϕ_0 axis, start at the bare substrate where $d = 0$ nm, point A, and end on the $D_{\phi 0}$ curve, point C. Equation (6) maps these lines of constant-angle-of-incidence to complete circles that trace the X plane unit circle, figure 2.4. Beginning at point A (+1, 0), it traces the unit circle clockwise until $d = D_{\phi 0}/2$ at point B (-1, 0). The X plane contour then continues clockwise until it ends at point C (C=A). Every constant angle of incidence line for a period of $D_{\phi 0}$ is

transformed into an X plane constant angle of incidence contour, XCAIC. After applying Eq. (3), the TEF bilinear transformation, these circles become τ plane constant angle of incidence contours, τCAICs. [1]

2.3.2 X Plane Constant-Thickness Contours (XCTCs)

Similarly, horizontal lines on the $\phi_0 - d_r$ plane drawn normal to the d axis can be drawn for any film thickness through the period of ϕ_0, from 0 to 90°. These horizontal lines of constant thickness are transformed by Eq. (6) to arcs of varying lengths on the X plane unit circle, XCTCs. The horizontal line where d = 0 nm on the $\phi_0 - d_r$ plane is transformed into a single point on the X plane, point A(+1, 0) on figure 2.4, for all angles of incidence. This is an infinite-to-one transformation. [1, 21] If a horizontal line of constant film thickness intersects the $D_{\phi_0}/2$ contour on the $\phi_0 - d_r$ plane then that point of intersection will be transformed to the point B on the X plane. In other words, every ordered pair (ϕ_0, d_r) that constitutes the $D_{\phi_0}/2$ contour is transformed to a single point B (-1, 0) on the X plane (figure 2.4); an infinite-to-one transformation. Likewise, every point of intersection on the D_{ϕ_0} curve is also transformed to a single point on the X plane, figure 2.4 point C (+1, 0). [1, 22]

Except for the two instances where horizontal lines of constant thickness intersect the $D_{\phi_0}/2$ and D_{ϕ_0} curves on the $\phi_0 - d_r$ plane, the parts of the horizontal line above the $D_{\phi_0}/2$ contour will be transformed into arcs in the positive X plane and the parts of the horizontal line the below $D_{\phi_0}/2$ contour will be transformed into arcs in the negative X plane. After applying Eq. (3) the TEF bilinear transformation, these arcs become constant thickness contours (τCTCs) on the τ plane. [1]

2.3.3 Film Thickness Subfamiles

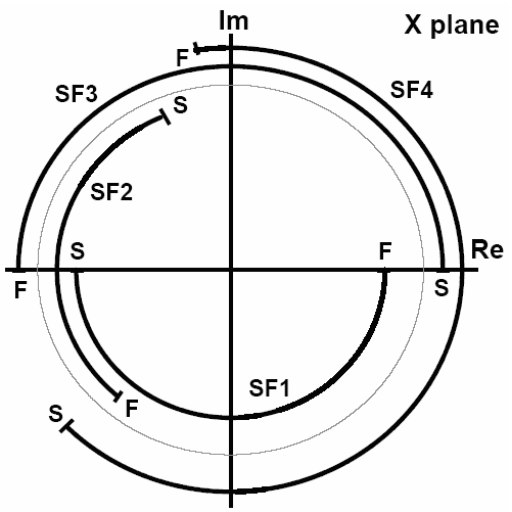

Figure 2.5: The X plane where $N_0 = 1.0$ and $N_1 = 1.46$ at λ=632.8 nm with subfamilies 1 through 4. Each arc represents all possible XCTCs for each subfamily from start (S) to finish (F). The ranges of XCTC SFs were derived from the film thickness ranges in figure 2.3.

As stated previously, lines of constant thickness on the $\phi_0 - d_r$ plane are transformed into arcs of varying lengths in the X plane. Real axis intersections of these XCTCs at (+1, 0) and (-1, 0) on the X plane allow us to further classify specific ranges of film thicknesses into subfamilies (SFs). [1] Figure 2.5 illustrates the full range of these arcs for each subfamily from start (S) to finish (F) where $N_0 = 1.0$ and $N_1 = 1.46$ at λ=632.8 nm. Subfamily 1 (SF1) includes the XCTCs that do not intersect the real axis and only reside in the negative imaginary half plane. Subfamily 2 (SF2) includes the XCTCs that intersect the real axis at X = B (-1, 0). Subfamily 3 (SF3) is similar to SF1 except it consists of all XCTCs that are in the positive imaginary half plane and do not intersect the real axis. Finally, subfamily 4 (SF4) includes the XCTCs that intersect the real axis at X = A (+1, 0). [1]

With this stated, ranges of film thickness from the $\phi_0 - d_r$ plane, figure 2.3, can be classified into their respective subfamilies:

- SF1 = $\left\{ d : 0 < d \le \frac{D_{0^\circ}}{2} \right\} = \left(0,\ D_{0^\circ} \right]$
- SF2 = $\left\{ d : \frac{D_{0^\circ}}{2} < d < \frac{D_{90^\circ}}{2} \right\} = \left(\frac{D_{0^\circ}}{2},\ \frac{D_{90^\circ}}{2} \right)$
- SF3 = $\left\{ d : \frac{D_{90^\circ}}{2} \le d \le D_{0^\circ} \right\} = \left[\frac{D_{90^\circ}}{2},\ D_{0^\circ} \right]$
- SF4 = $\left\{ d : D_{0^\circ} < d \le D_{90^\circ} \right\} = \left(D_{0^\circ},\ D_{90^\circ} \right]$

2.4 COMPLEX τ PLANE

The TEF is related to the exponential film thickness function by a bilinear transformation. [21] It successively transforms constant-angle-of-incidence lines and constant-thickness lines from the $\phi_0 - d_r$ plane to XCAICs and XCTCs on the unit circle in the X plane, respectively. It then transforms these X plane XCAICs and XCTCs to τ plane τCAICs and τCTCs, respectively.

2.4.1 τ Plane Constant-Angle-of-Incidence Contours (τCAICs)

The X plane to τ plane transformation maps XCAICs to τCAICs, circles to circles, Eq. (3). When the angle of incidence $\phi_0 = 0°$ the τCAIC is a circle with a radius of 0; a point at $\tau = +1$. As the angle of incidence is increased a circle on the τ plane is traced with an increased radius. These τCAICs begin on the real axis where $d = 0$ nm and rotate clockwise as the film thickness is increased. When $d = D_{\phi_0}/2$ a semi-circle is traced as the τCAIC passes through the real axis at $\tau < 1$ for the negative, $\tau = 1$ for the zero, and $\tau > 1$

for the positive film-substrate systems; figures 2.6, 2.7(a), and 2.7(b) respectively. As the film thickness is increased further, the τCAIC continues clockwise, terminating at its point of origin on the real axis, when $d = D_{\phi_0}$, figures 2.6 and 2.7. The largest τCAIC for all systems occurs when $\phi_0 = 90°$, τCAIC(90). [1]

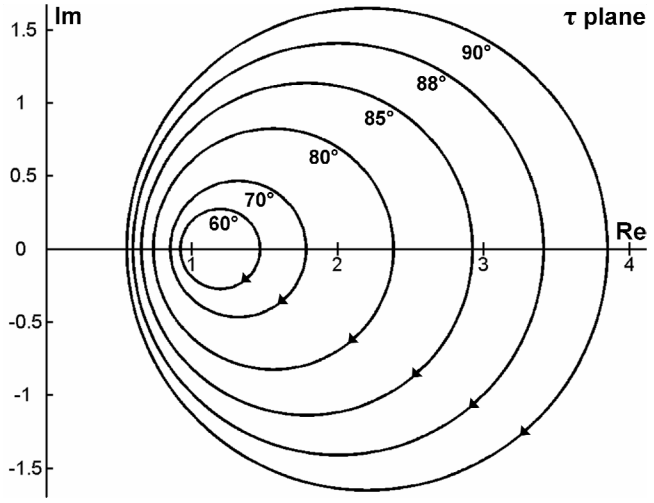

Figure 2.6: Negative film-substrate system τCAICs for $\phi_0 = 60$, 70, 80, 88, and 90° where N_1 (N_2) = 1.46 (3.85) at λ=632.8 nm. Each negative system τCAIC begins on the real axis where $\tau \geq 1$.

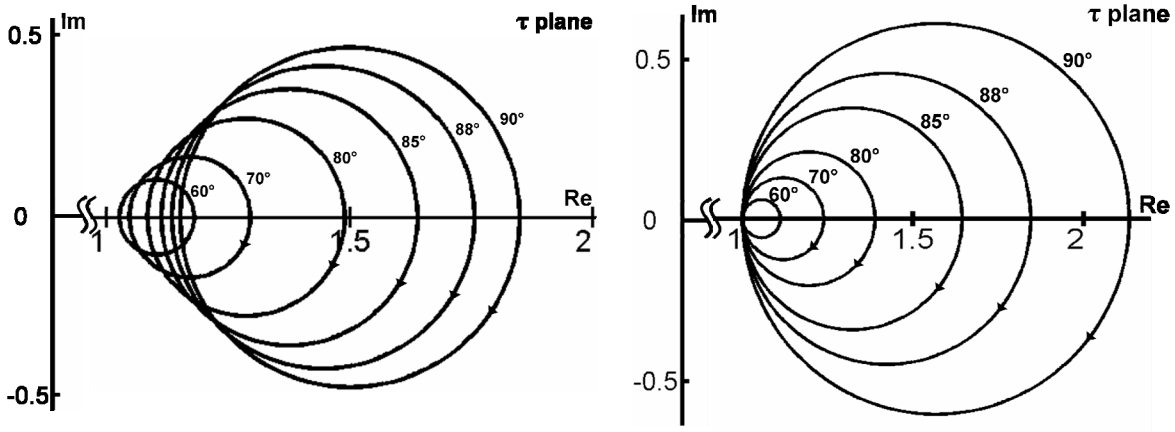

(a) (b)

Figure 2.7: (a) Zero and (b) Positive film-substrate system τCAICs for $\phi_0 = 60$, 70, 80, 88, and 90° where N_1 (N_2) = 1.46 (2.1316) and 1.46 (1.85), respectively at λ=632.8 nm. Each systems τCAICs begin on the real axis where $\tau \geq 1$.

2.4.2 τ Plane Constant-Thickness Contours (τCTCs)

Regardless of the film substrate system's category, negative, zero, or positive, all τCTCs exhibit a similar general behavior. XCTC arcs are transformed to the τ plane through the bilinear transformation of Eq. (3). The (+1, 0) point on the X plane where d = 0 nm for all angles of incidence is transformed to a contour on the τ plane that traces the real axis. This zero thickness contour begins at the point τ = (+1, 0) when $\phi_0 = 0°$ and ends at $\tau = N_2/N_0$ when $\phi_0 = 90°$. As the film thickness is increased, the τCTC subfamily behavior is classified by the XCTCs intersection with the X plane real axis, see section 2.3.3. [1, 22]

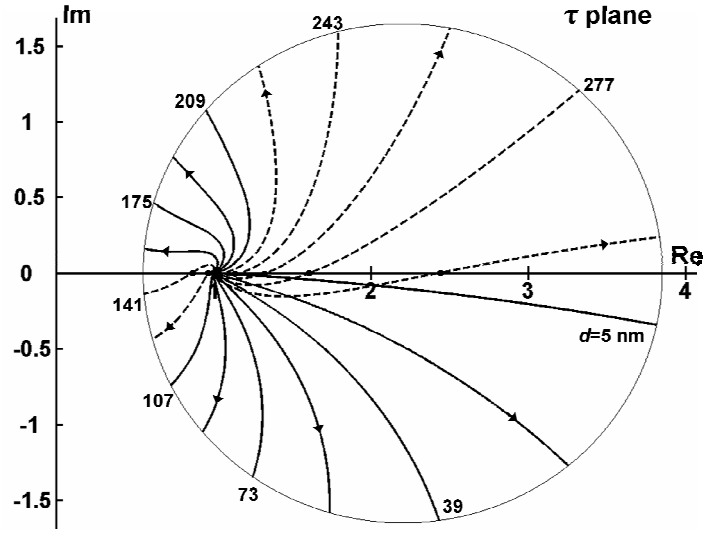

Figure 2.8: Negative film-substrate system τCTCs for N_1 (N_2) = 1.46 (3.85) at λ=632.8 nm. All four subfamilies are shown with film thickness labeled. (Clockwise - SF1: solid τCTCs in negative imaginary half plane. SF2: dashed τCTCs ending in negative imaginary half plane. SF3: solid τCTCs in positive imaginary half plane. SF4: dashed τCTCs ending in positive imaginary half plane.)

SF1 XCTCs do not intersect the real axis and exist in the negative imaginary X plane. They are transformed to the τ plane as SF1 τCTCs, such that they start at the point (+1, 0)

and are projected into the negative imaginary τ plane. This can be seen in figures 2.8 and 2.9 as long solid contour lines in the negative imaginary half plane. [1, 22]

SF2 XCTCs have both positive and negative imaginary components because they intersect the X plane real axis at the point (-1, 0). This intersection occurs when the ordered pair $(\phi_0, d_r) = (\phi_0, D_{\phi 0}/2)$. These SF2 XCTCs are transformed into SF2 τCTCs with similar traits. They begin on the τ plane at the point (+1, 0) and travel into the positive imaginary half plane. When $(\phi_0, d_r) = (\phi_0, D_{\phi 0}/2)$, the SF2 τCTC curves back to intersect the real axis at a point determined by the film-substrate system's category. If the system is negative as in figure 2.8, the SF2 τCTC intersects the real axis at $\tau < 1$. If the system is zero, figure 2.9(a), the intersection occurs at $\tau = 1$, and if the system is positive, figure 2.9(b), the intersection occurs at $\tau > 1$. After its real axis intersection, the SF2 τCTC continues into and terminates in the negative imaginary half plane. [1, 22]

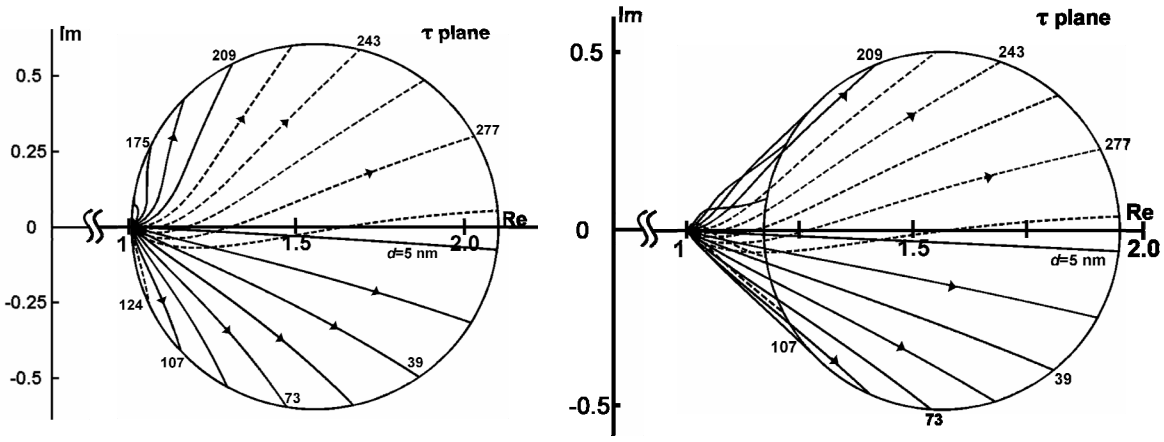

Figure 2.9: τCTCs of the (a) zero and (b) positive film-substrate systems for N_1 (N_2) = 1.46(2.1316) and 1.46(1.85) at λ=632.8 nm, respectively. (Clockwise - SF1: solid τCTCs in the negative imaginary half plane. SF2: short dashed τCTCs ending in negative imaginary half plane. SF3: solid τCTCs in positive imaginary half plane. SF4: long dashed τCTCs ending in positive imaginary half plane.)

SF3 XCTCs do not intersect the real axis in the X plane and reside in the positive imaginary half plane. As a result, SF3 τCTCs begin at the point (+1, 0) and are only projected into the positive imaginary half plane, without ever intersecting the real axis as seen in figure 2.7 as the solid contours in the positive imaginary half plane. [1, 22]

SF4 XCTCs are similar to SF2 XCTCs except they intersect the X plane real axis at the point (+1, 0), not (-1, 0). When transformed to the τ plane, SF4 τCTCs start at the point (+1, 0) and travel into the negative imaginary half plane, intersect the real axis when (ϕ_0, d_r) = (ϕ_0, $D_{\phi 0}$) at τ > 1 for all three systems, negative, zero, and positive. After its real axis intersection, the SF4 τCTC continues into and terminates in the positive imaginary half plane. [1, 22] This can be seen on figures 2.8 and 2.9 by the longer dashed contours terminating in the positive imaginary half plane.

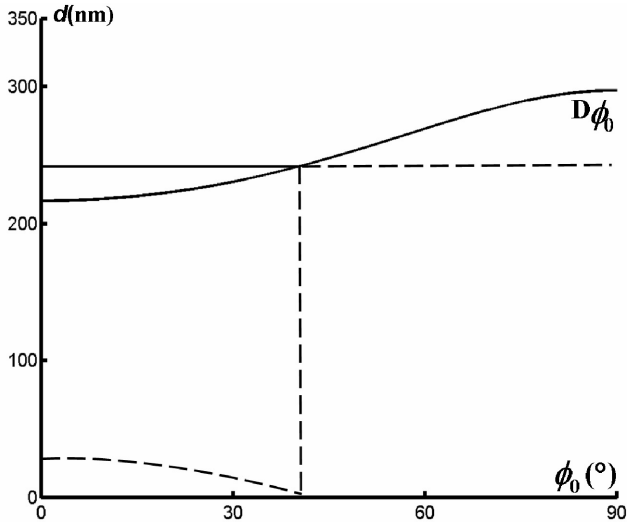

Figure 2.10: The $\phi_0 - d_r$ plane with a horizontal line of constant thickness in SF4. The portion of the constant thickness line (solid) is above the $D_{\phi 0}$ curve and therefore outside of the $\phi_0 - d_r$ plane. This portion of the constant thickness line is projected onto the $\phi_0 - d_r$ plane as an image and transformed as an image overlapping the SF2 τCTC in the negative imaginary half plane until $d = D_{\phi 0}$. The remainder of the line is within the $\phi_0 - d_r$ plane and is transformed into a τCTC in the positive imaginary half plane.

The part of the SF4 τCTCs that overlap other subfamilies in the negative imaginary half plane is an image. Figure 2.10 shows that the horizontal line in the range of the D_{ϕ_0} curve is discontinuous at $d = D_{\phi_0}$ where the film-substrate acts as a bare substrate. When the SF4 ordered pair is above the D_{ϕ_0} curve on the $\phi_0 - d_r$ plane, it is not part of the reduced film thickness $\phi_0 - d_r$ plane. It is projected onto the negative half plane as an image overlapping other subfamilies. When the ordered pair is below the D_{ϕ_0} curve (ϕ_0, $d \leq D_{\phi_0}$), it is in the reduced film-thickness plane and the SF4 τCTCs are transformed to the positive imaginary half plane. [1, 22]

CHAPTER III
THE SMITH CHART

3.1 INTRODUCTION

The Smith chart was developed by Philip H. Smith at Bell Telephone's Radio Research Lab and was first published in 1939. [10] It is used as a graphical aid for simplifying the complex mathematics needed to describe characteristics of microwave components. [23, 24]

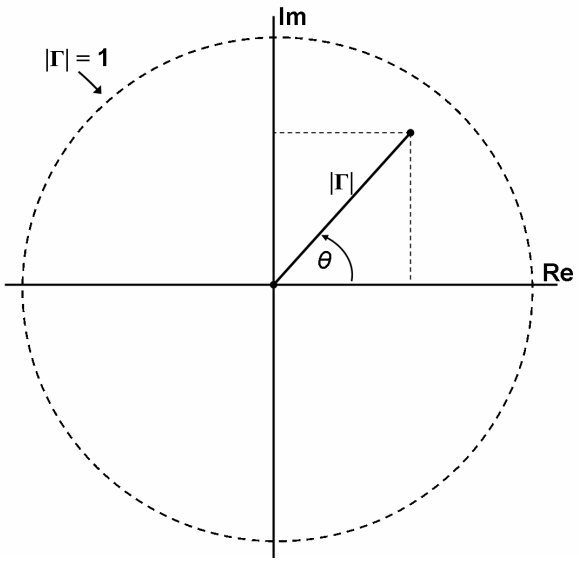

Figure 3.1: The complex reflection plane.

It is derived from the complex nature of the transmission line wave reflection coefficient, Γ, written as

$$\Gamma = \frac{V_r}{V_i}, \qquad (10)$$

which is a ratio of the reflected voltage amplitude, V_r, to the incident voltage amplitude, V_i. This reflection is usually caused by an impedance mismatch between the characteristic

impedance of the line Z_0, and the impedance of the load Z_L. The characteristic impedance is a real value when the transmission line is lossless and the load impedance is generally composed of inductive or capacitive traits, making it complex. Equation (10) can be rewritten in the form [19]

$$\Gamma = \frac{Z_L - Z_0}{Z_L + Z_0}, \tag{11}$$

as a function of the characteristic impedance of the line and the impedance of the load. Normalizing Eq. (11) to the characteristic impedance Z_0, yields

$$\Gamma = \frac{z_L - 1}{z_L + 1}, \tag{12}$$

where the normalized complex load impedance is expressed as the sum of a resistance *r* and reactance *x* as

$$z_L = r + jx. \tag{13}$$

The relationship of Eq. (12) between the normalized complex load impedance z_L and the reflection coefficient Γ is a bilinear transformation. This means that for every z_L there is one and only one Γ, and for every Γ there is one, and only one z_L. This allows for the transformation of the complex rectangular impedance plane, [25] to the polar complex reflection plane of figure 3.1. [11] It is this bilinear transformation that yields the two families that make up the Smith chart; the constant resistance contours and the constant reactance contours.

Given a lossless passive device, the experienced wave reflection will have a magnitude equal to or less than 1. Therefore, the largest reflection must lie on the unit circle of the complex plane for any relative phase angle and the domain of the Smith chart must lie on

or inside this unit circle. [11] By rewriting Eq. (13) in terms of Eq. (12), the real and imaginary parts can be separated to [24]

$$r = \frac{1-\Gamma_r^2-\Gamma_i^2}{\left(1-\Gamma_r\right)^2+\Gamma_i^2}, \tag{14}$$

and

$$x = \frac{2\Gamma_i}{\left(1-\Gamma_r\right)^2+\Gamma_i^2}, \tag{15}$$

where the reflection coefficient can be written in terms of its real Γ_r and imaginary Γ_i parts as

$$\Gamma = \Gamma_r + j\Gamma_i \tag{16}$$

After some algebraic manipulation, [24] Eqs. (14) and (15) can be written as equations for circles on a complex plane representing the transformation of lines of constant resistance

$$\left(\Gamma_r - \frac{r}{1+r}\right)^2 + \Gamma_i^2 = \left(\frac{r}{1+r}\right)^2 \tag{17}$$

and the transformation of lines of constant reactance

$$\left(\Gamma_r - 1\right)^2 + \left(\Gamma_i - \frac{1}{jx}\right)^2 = \left(\frac{1}{jx}\right)^2 \tag{18}$$

For clarification, the equation for a circle is

$$(x - h)^2 + (y - k)^2 = \text{radius}^2 \tag{19}$$

where h and k are the x- and y-coordinates of the center of the circle.

3.2 CONSTANT-RESISTANCE CONTOURS

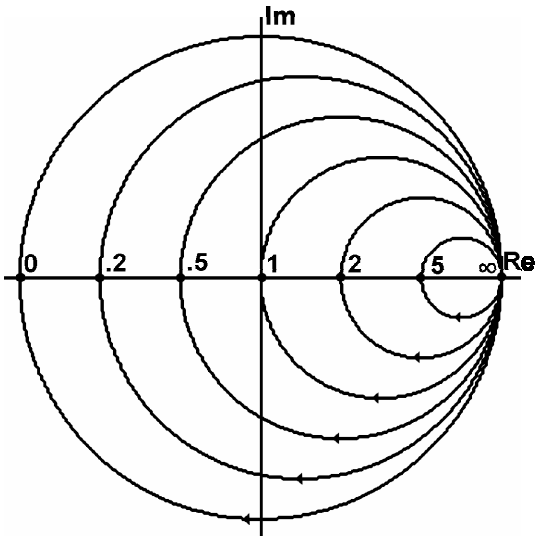

Figure 3.2: Constant-resistance contours and the unit circle. Each circle represents a single value of real resistance as the reactance is increased from negative to positive infinity. When the resistance = 0, the resistance contour traces the unit circle. As the resistance is increased, the contour's diameter becomes smaller until that of the resistance = ∞ collapses to the point (+1, 0).

A constant-resistance contour (circle), as illustrated in figure 3.2, represents the same resistance r value at every point on that circle for a changing reactance x from – to + ∞. All contours pass through the point (+1, 0) on the complex plane and each of their centers lie on the real axis. The largest contour represents a resistance value $r = 0$. For clarification, by substituting $r = 0$ into Eq. (12), $\Gamma = -1$, $|\Gamma|=1$, and the constant resistance contour lies on the unit circle. Conversely, when r = ∞, $\Gamma= +1$, $|\Gamma|=1$, and the constant resistance contour is the point (+1, 0). [11, 24]

3.3 CONSTANT-REACTANCE CONTOURS

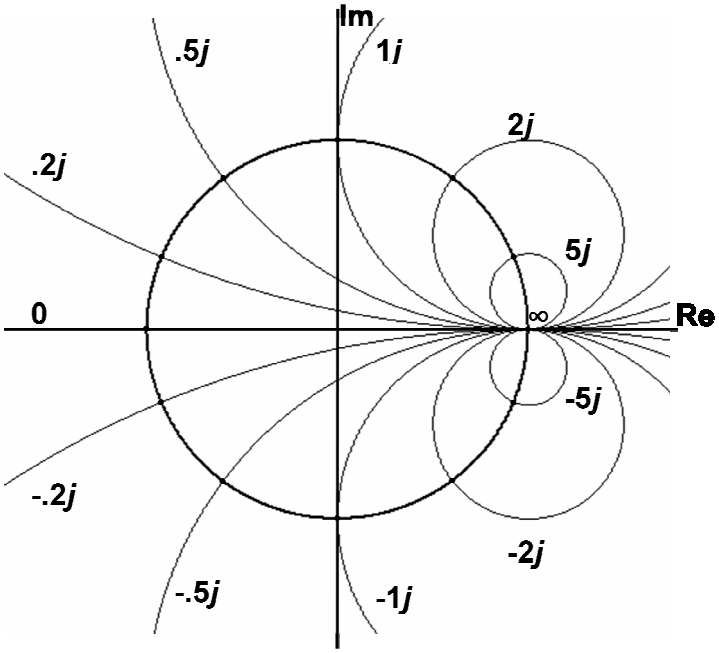

Figure 3.3: Constant-reactance contours superimposed onto the complex plane with the unit circle. Each contour represents a single value of reactance as the resistance is increased from 0 to ∞.

A constant reactance contour (arc) from Eq. (18) represents the same reactance value at every point on that circle as the resistance is increased from 0 to ∞. All reactance circles pass through the real axis at the point (+1, 0) on the complex plane. Their radius is $1/x$ and their centers are located along the axis of $(1, 1/x)$. The circle where the reactance is zero, $1/x = \infty$, is represented by the real axis as a circle of infinite radius. Similarly, when the reactance is infinity then $1/x = 0$, the constant reactance contour is the point (+1, 0) on the real axis. The reactance contours in the positive imaginary half plane are inductive, whereas contours in the negative imaginary half plane are capacitive. [24] In compliance with the domain of the Smith chart, only the portions of the reactance contours, arcs, that are inside the unit circle are relevant when considering passive impedance. [11, 24, 25]

3.4 COMBINED REFLECTANCE AND IMPEDANCE PLANES

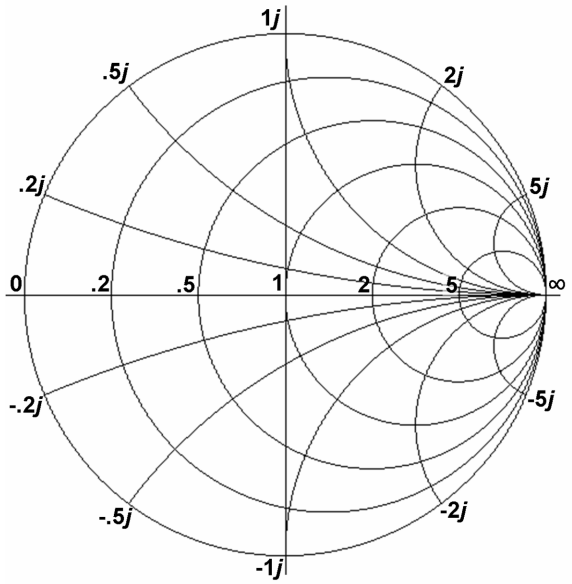

Figure 3.4: The Smith chart. Constant resistance contours and constant reactance contours superimposed on the unit circle of the complex plane..

When both the resistance circles and reactance arcs are plotted together, bound by the unit circle, the Smith chart emerges. Every intersection of a resistance and reactance contour represents a unique normalized impedance value, transformed from the rectangular complex impedance plane. The center of the Smith chart is called the prime center. It is assigned the value of the transmission line characteristic impedance, Z_0, and allows the entire chart to be normalized. This makes the chart more user-friendly because the center will always have the value of 1.0. [23]

Just as the rectangular complex impedance plane is symmetric about the real axis, so is the Smith chart. A value of impedance in one plane, either positive or negative, will have a complex conjugate in the opposing plane of equal magnitude and opposite angle from the prime center. [11]

3.5 THE ADMITTANCE CHART

Just as the Smith chart is formed by constant resistance and constant reactance contours, the Admittance chart is made by plotting constant conductance and constant susceptance contours, figure 3.5. It is normalized by dividing by the inverse of the characteristic impedance. Essentially, by mirroring the Smith chart, or flipping it on the imaginary axis, every impedance value on the Smith chart can also be represented by its inverse of 1/Z. A significant amount of research has been conducted on the Admittance chart, its use, and applications. More details are in references [26-28].

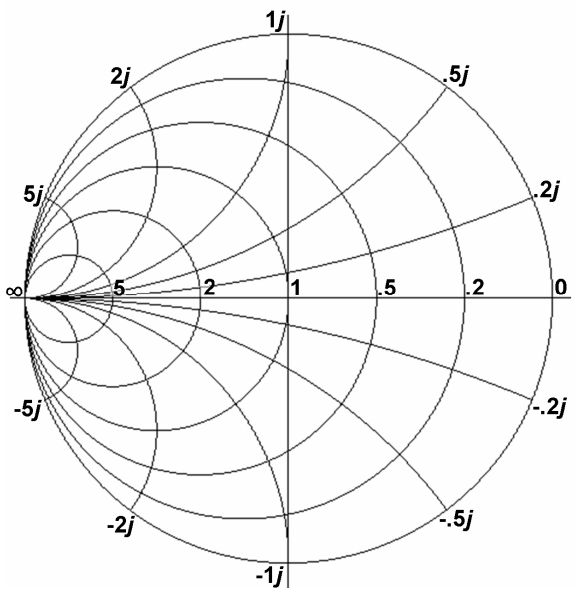

Figure 3.5: The Admittance chart superimposed onto the complex plane and bound by the unit circle.

CHAPTER IV
COMPARISON OF τCAICS AND τCTCS OF THE TRANSMISSION ELLIPSOMETRIC FUNCTION WITH THE SMITH CHART

4.1 INTRODUCTION

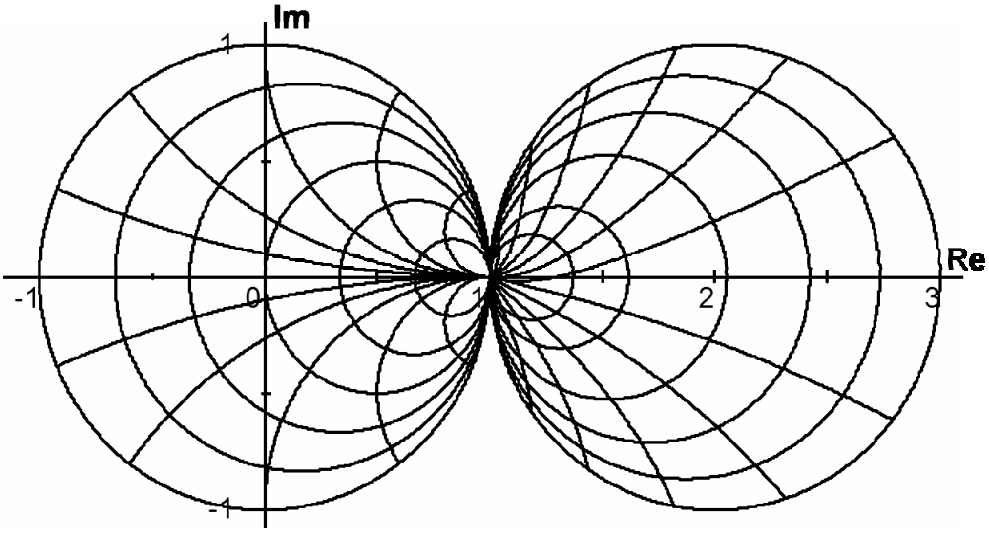

Figure 4.1: The Smith chart and a zero film-substrate system where N_1 (N_2) = 2.0 (4.0) at λ=632.8 nm plotted on the same complex plane.

The following is a comparative analysis of the Smith chart and the constant-thickness contours/constant-angle-of-incidence contours of the transmission ellipsometric function. Both the film and substrate are assumed to be semi-infinite parallel planes of transparent, isotropic, and non-absorbing mediums. Figure 4.1 shows the Smith chart and the τCAICs and τCTCs of a zero film-substrate system plotted together on the same complex plane.

4.2 FILM-SUBSTRATE SYSTEM CATEGORIES

The three categories of film-substrate systems are negative, zero, and positive. A

system is classified as negative if $N_1 < \sqrt{N_0 \cdot N_2}$, zero if $N_1 = \sqrt{N_0 \cdot N_2}$, and positive if $N_1 > \sqrt{N_0 \cdot N_2}$. Figures 4.2 - 4.4 demonstrate the general behavior for each of these categories. Each system is plotted using a transparent (lossless) film on a transparent (lossless) substrate. In order to maintain relative uniformity between categories, each system uses the same film index (N_1=1.46) and only the substrate is varied to meet the desired condition. These figures are left primarily unlabeled because we are currently only interested in the systems general behavior.

4.2.1 Negative Film-Substrate System

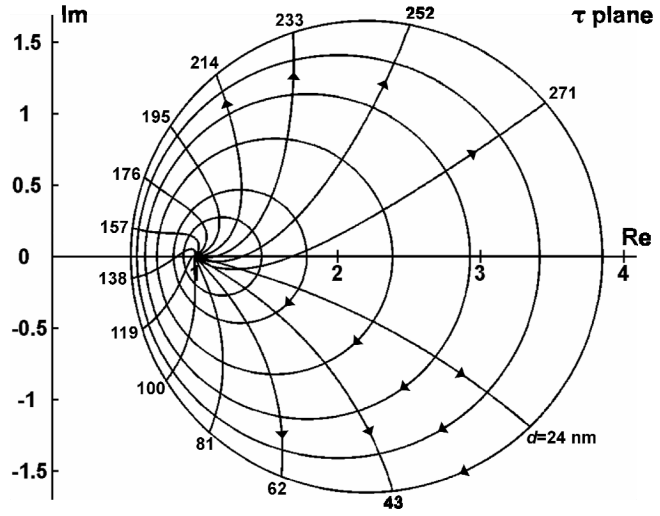

Figure 4.2: Negative film-substrate system in the τ plane. N_1 (N_2) = 1.46 (3.85) at λ=632.8 nm. The τCAICs are plotted for ϕ_0 = 60, 70, 80, 88, and the largest at 90°. This is a non-normalized system.

The negative film-substrate system, figure 4.2, like the Smith chart, is a single-valued system. Every point within the τCAIC(90) represents a single ordered pair from the $\phi_0 - d_r$ plane. Unlike the Smith chart's the constant resistance circles, the negative film-substrate

system's τCAICs do not intersect each other at a single common point. For this reason, the negative system will not be used in the comparison with the Smith chart contours discussed in chapter 3. However, it does appear similar to Phillip Smith's initial transmission line calculator (circa 1931), figure A.1 which was not normalized to encompass all possible values of impedance. [11] A comparison of the negative film-substrate system and Smith's initial transmission line calculator will be presented elsewhere.

4.2.2 Zero Film-Substrate System

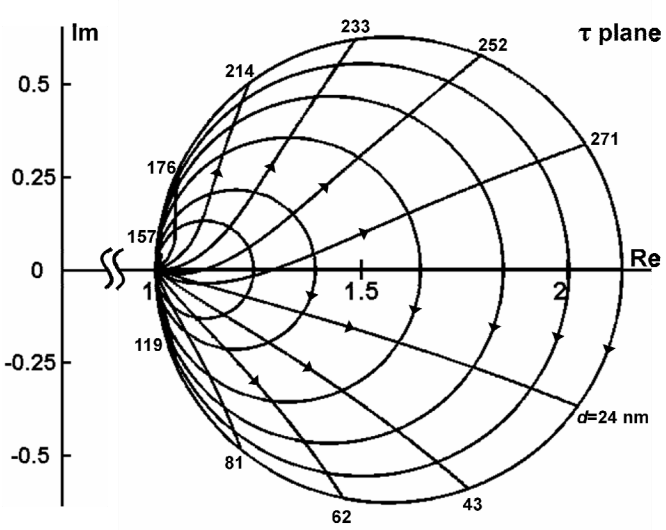

Figure 4.3: Zero film-substrate system in the τ plane. N_1 (N_2) = 1.46 (2.1316) at λ=632.8 nm. The τCAICs are plotted for ϕ = 60, 70, 80, 88, and the largest at 90°. This is a non-normalized system.

The zero film-substrate system, figure 4.3, has distinct similarities with the Smith chart. It is bound by the τCAIC(90) which can be filled by tangential circles that intersect one another at the single common point (+1, 0). The Smith chart is bound by a constant resistance contour that traces the unit circle. It is filled by smaller tangential constant-resistance contours that intersect at the single common point (+1, 0) as well. This point of

(+1, 0) represents an infinite-to-one transformation in both the τ plane zero film-substrate system as well as the Smith chart. All other points within the τCAIC(90) and the unit circle represent a one-to-one transformation.

The zero film-substrate systems τCAICs and τCTCs will be the only system used throughout this thesis for the comparison with the Smith chart contours.

4.2.3 Positive Film-Substrate System

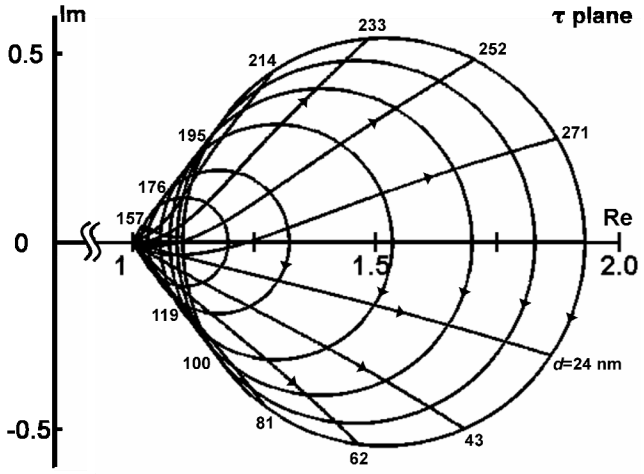

Figure 4.4: Positive film-substrate system in the τ plane. N_1 (N_2) = 1.46 (1.85) at λ=632.8 nm. The τCAICs are plotted for ϕ = 60, 70, 80, 88, and the largest at 90°. This is a non-normalized system.

By inspection, the positive film-substrate system, figure 4.4, is seen to have overlapping τCAICs. This behavior allows for specific values of τ to be satisfied at two separate angles of incidence, making it a double-valued system. [22] This is a direct contradiction to the Smith chart's one-to-one bilinear transformation condition. Hence, the positive film-substrate system is not a comparable candidate to the Smith chart.

4.3 ORDERED PAIR PLANE

Many of the similarities and differences between the τ plane contours and Smith chart contours are deeply rooted within their respective planes of origin; the $\phi_0 - d_r$ plane and the rectangular complex impedance plane. Comparing these two planes of origin results in a better understanding of the upcoming contour comparisons.

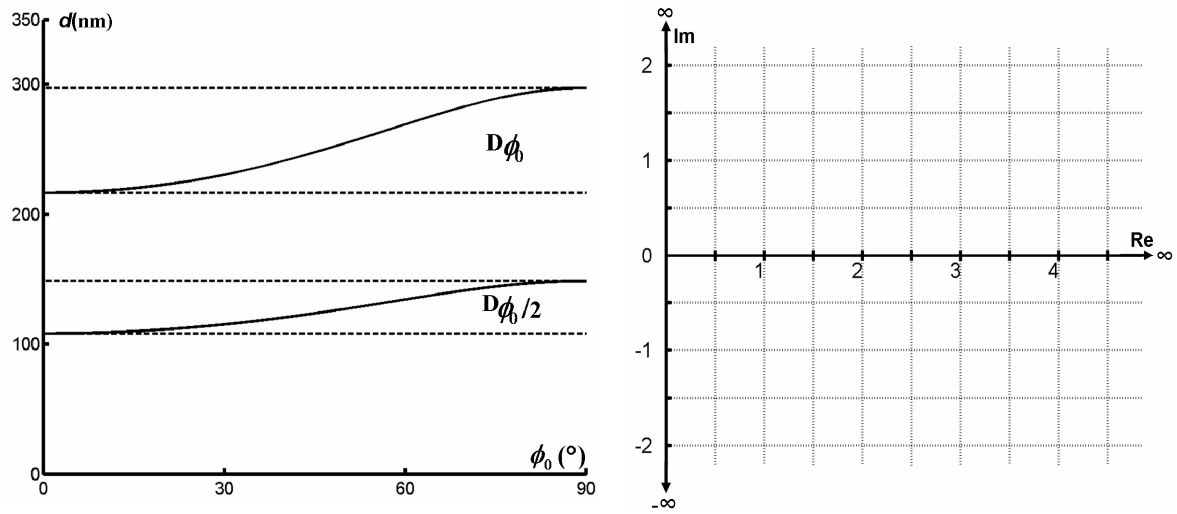

(a) (b)

Figure 4.5: The planes of origin. (a) The $\phi_0 - d_r$ plane for a film-substrate system where $N_1/N_0 = 1.46$. The horizontal dotted lines mark the range of film thickness for the upper boundary, $D_{\phi 0}$, and bisecting contour, $D_{\phi 0}/2$. (b) The rectangular complex impedance plane whose three boundaries extend to infinity.

4.3.1 The $\phi_0 - d_r$ Plane

The $\phi_0 - d_r$ plane, figure 4.5(a), is a non-complex plane composed of all ordered pairs that fill the domain of a zero film-substrate system on the τ plane. The ϕ_0 axis is bound by linear vertical finite boundaries where $\phi_{0(min)} = 0°$ and $\phi_{0(max)} = 90°$. The d axis is bound below by the minimum film thickness where $d_{r(min)} = 0$ nm (bare substrate) and the non-linear $D_{\phi 0}$ curve above where $d_{r(max)} = D_{\phi 0}$. Although not readily apparent, the $\phi_0 - d_r$ plane is bisected into two equal areas by the $d = D_{\phi 0}/2$ contour as proved below:

If the total area under $\phi_0 - d_r$ plane D_{ϕ_0} curve is (D) where $D = \int_0^{90} D_{\phi_0}\, d\phi_0$ and the area under the $\phi_0 - d_r$ plane $\frac{D_{\phi_0}}{2}$ curve is (E) where $E = \int_0^{90} \frac{D_{\phi_0}}{2}\, d\phi_0$, then the area between the D_{ϕ_0} curve and the $\frac{D_{\phi_0}}{2}$ curve is (F) or the difference between (D) and (E) where

$$F = \int_0^{90} D_{\phi_0}\, d\phi_0 - \int_0^{90} \frac{D_{\phi_0}}{2}\, d\phi_0 = \int_0^{90} \left(D_{\phi_0} - \frac{D_{\phi_0}}{2} \right) d\phi_0 = \int_0^{90} \frac{D_{\phi_0}}{2}\, d\phi_0$$

$$\therefore F = E .$$

Therefore the $D_{\phi 0}/2$ contour bisects the $\phi_0 - d_r$ plane into two equal areas. Additionally, the $\phi_0 - d_r$ plane is non-complex in nature.

4.3.2 The Rectangular Complex Impedance Plane

The rectangular complex impedance plane, figure 4.5(b), is composed of all ordered pairs of impedance values (x, y) = (resistance, reactance). [25] It is a complex plane, bound by the real and imaginary axes where $Re_{(min)} = 0$, $Re_{(max)} = +\infty$, $Im_{(min)} = -\infty$, and $Im_{(max)} = +\infty$. The real axis bisects the impedance plane and divides it into two symmetric positive and negative imaginary halves. Every point on the plane has a complex conjugate in the opposing plane.

4.3.3 Planes of Origin Comparison

In comparison, the $\phi_0 - d_r$ plane is completely real, whereas the rectangular impedance plane is complex. This does not cause significant discrepancies because every ordered pair in the $\phi_0 - d_r$ plane is successively transformed to the complex X plane (see section 2.3) by the complex exponential film thickness function X and then to the complex τ plane by the bilinear transformation of Eq. (3).

The complex rectangular impedance plane is linearly bound on all 4 sides, 3 of which extend to infinity. The $\phi_0 - d_r$ plane is linearly bound on three of its four sides where its fourth and upper boundary is dictated by the film-thickness function, $D_{\phi 0}$; Eq. (9).
As the real axis divides the impedance plane into two symmetric rectangular imaginary (positive and negative) half planes of complex conjugates, the $\phi_0 - d_r$ plane is bisected by the $D_{\phi 0}/2$ curve into two non-symmetric, equal areas. The non-linear behavior of the $D_{\phi 0}$ ($D_{\phi 0}/2$) boundary (bisector) results in the greatest difference between the Smith chart and the zero system τ plane contours. The Smith charts symmetry is a direct result of the linear boundaries of its plane of origin. The τ plane contours do not share this symmetry because of the non-linearity of its boundaries.

4.4 PLANE TRANSFORMATIONS

4.4.1 Transmission Ellipsometric Function Transformation

$$\tau = a \cdot \frac{1 + bX}{1 + cX} \tag{3}$$

The transmission ellipsometric function (TEF), Eq. (3), is the product of a bilinear transformation of the Fresnel reflection coefficients and a coefficient composed of the ratio of Fresnel coefficients for transmission. Through two successive transformations, the TEF maps the set of all ordered pairs (ϕ_0, d_r) of a film-substrate system to the complex τ plane.

Vertical lines of constant-angle-of-incidence ϕ_0 on the $\phi_0 - d_r$ plane are completely mapped to full circles on the X plane, XCAICs. These XCAICs are then transformed to constant-angle-of-incidence contours, τCAICs, on the τ plane in a one-to-one mapping. [1] Where $\phi_0 = 0°$, all film thicknesses undergo an infinite-to-one transformation to the point

(+1, 0) on the X plane and the τCAIC(0) is a single point on the τ plane at (+1, 0), singularity point. [22] As ϕ_0 is increased, the radius of the τCAICs increases until it reaches the largest τCAIC at 90°, τCAIC(90). The TEF also transforms every point on the $\phi_0 - d_r$ plane where $d = D_{\phi 0}/2$, to the single X plane point (-1, 0) and subsequently, to a single point on the real axis of the τ plane (+1, 0), an infinite-to-one transformation. [1]

4.4.2 Smith Chart Transformation

$$\Gamma = \frac{z_L - 1}{z_L + 1} \qquad (12)$$

The Smith chart is completely derived from Eq. (12) which is a bilinear transformation that maps the entire complex rectangular impedance plane into the unit circle on the polar impedance plane (the complex plane), point by point, a one-to-one transformation. Lines of constant-resistance and constant-reactance are transformed into contours of constant-resistance and constant-reactance, respectively. Because the Smith chart represents passive impedances, the largest value of passive reflection is Γ = 1, see section 3.1.

As previously stated, three of four limits on the rectangular impedance plane extend to infinity. When these limits of infinity undergo the bilinear transformation, an infinite-to-one transformation takes place and these limits are all transformed to the single point (+1, 0) on the Smith chart.

4.4.3 Plane Transformation Comparison

Both planes of origin are transformed by their respective bilinear transformations. The TEF successively transforms the real $\phi_0 - d_r$ plane into the complex τ plane through the complex X plane. The rectangular impedance plane is already complex and is simply

transformed to the polar complex impedance plane.

Vertical lines of constant value from both planes of origin are transformed into full circles (contours) in their respective τ and impedance plane. These transformed circles also begin and end on the real axis in both cases, where the circle's starting point coincides with the respective lower limit of their plane of origin and the ending points coincide with the upper limit on their planes of origin. The mid-point for each transformed circle is the midpoint for the vertical line of constant value. Both of these mid-points are transformed to the real axis at their circles' diameter. This occurs anywhere between +/- 1 on the complex impedance plane and at the single point (+1, 0) on the τ plane.

Similarly, horizontal lines of constant value from both planes of origin are transformed into contours on the τ plane and Smith chart, respectively. The interaction of these horizontal lines with their respective plane of origin bisector determines its general behavior after transformation. To clarify, the $D_{\phi_0}/2$ contour bisects the $\phi_0 - d_r$ plane and the real axis bisects the complex impedance plane. For example, a horizontal line below, but not intersecting, its plane of origin bisector is transformed to the negative imaginary half plane. A horizontal line above, but not intersecting, its plane of origin bisector is transformed to the positive imaginary half plane. But, if the horizontal line from the plane of origin intersects its planar bisector, the portion above (below) is transformed to the positive (negative) imaginary half plane and the point of intersection is transformed to the point (+1, 0). This condition is only applicable to the τ plane transformation due to the non-linear behavior of the $D_{\phi_0}/2$ curve. The rectangular complex impedance plane's bisecting line (the real axis) does not have a positive or negative imaginary part and is therefore only transformed to the real axis.

With only one exception, both bilinear transformations perform a complete one-to-one mapping from their planes of origin to its corresponding complex planes. The exception is an infinite-to-one transformation to the point (+1, 0). For the TEF, this occurs for any film thickness at 0° angle-of-incidence and when $d = D_{\phi_0}/2$ for any angle of incidence on the $\phi_0 - d_r$ plane. Similarly, for the Smith chart, this occurs when any impedance value is equivalent to infinity. In either case, the transformation is to the single common point (+1, 0).

4.5 TANGENTIAL CIRCLES

4.5.1 τ Plane Constant-Angle-of-Incidence Contours (τCAICs)

Vertical lines of constant-angle-of-incidence on the $\phi_0 - d_r$ plane are transformed into constant-angle-of-incidence contours, τCAICs, on the τ plane, figure 4.6(a). The $\phi_0 = 0°$ τCAIC, τCAIC(0), is the smallest τCAIC having a radius of zero at the point (+1, 0). As the angle of incidence is increased the radius of the τCAIC is also increased. Each τCAIC begins on the real axis at $\tau \geq 1$ where $d = 0$ nm. By holding ϕ_0 constant and increasing the film thickness, the τCAIC traces a clockwise circle. When the film thickness reaches $d = D_{\phi_0}/2$, the τCAIC completes a semi-circle in the negative imaginary half plane and intersects the real axis at the point (+1, 0). This intersection with the real axis occurs at a single point (+1, 0) for all ordered pairs of (ϕ_0, $D_{\phi_0}/2$) when transformed to the τ plane; figure 4.6(a). As the film thickness d is increased from $D_{\phi_0}/2$ to D_{ϕ_0}, the τCAIC continues clockwise into the positive imaginary half plane. The τCAIC is complete when $d = D_{\phi_0}$ where it reaches the real axis at the same point that it began at, ending the first period of mD_{ϕ_0} ($m = 1$) and beginning the next period ($m = 2$); refer to figure 2.2.

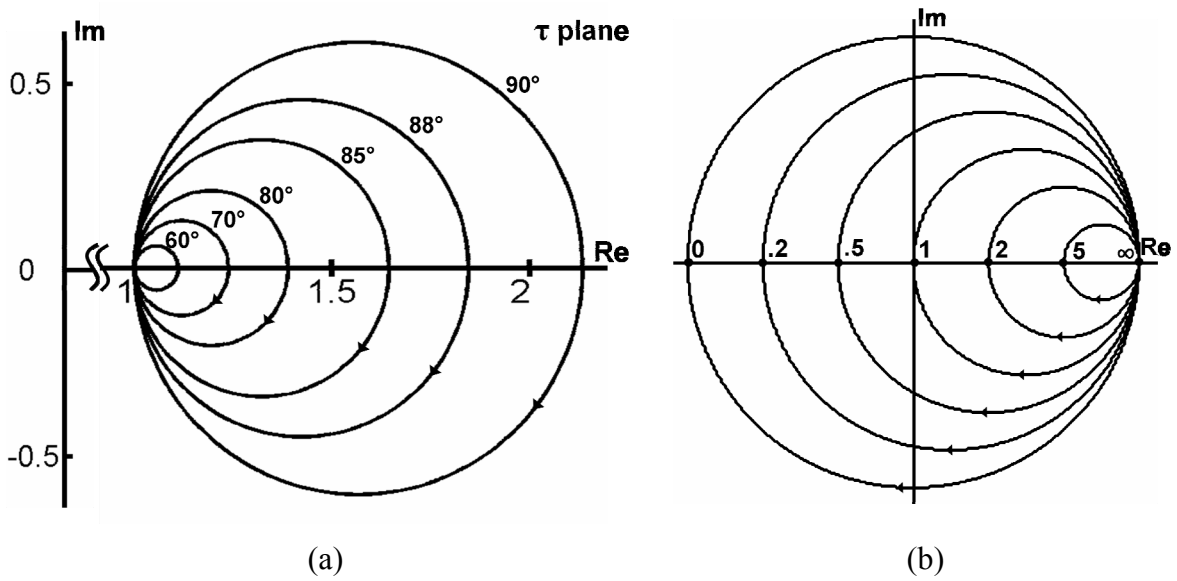

(a) (b)

Figure 4.6: (a) Tangential τCAICs in the τ plane and (b) tangential constant-resistance circles on the Smith chart superimposed onto the complex plane with the unit circle.

The largest τCAIC occurs when $\phi_0 = 90°$, τCAIC(90), and all other τCAICs are included within it where τCAIC($\phi_0 < 90$). Each τCAIC is a one-to-one transformation from the $\phi_0 - d_r$ plane to the τ plane where $d \neq D_{\phi 0}/2$. When $d = D_{\phi 0}/2$ an infinite-to-one transformation exists to the single point (+1, 0). This is a singularity point. [22] Because all τCAICs are centered on the same axis and intersect at a single common point, they are tangential to one another at this point, (+1, 0) figure 4.6(a).

4.5.2 Smith Chart Constant-Resistance Contours

Vertical lines on the complex impedance plane intersect the real axis only once. They are transformed into full circles called constant-resistance contours on the Smith chart. Each contour represents a normalized value of resistance where the vertical line intersected the real axis as it traveled from $\pm j$ infinity on the rectangular plane. For example, the imaginary axis of the rectangular complex impedance plane intersects the real axis at a

value of zero resistance, figure 4.5(b). This vertical line is transformed into the largest circle of the Smith chart which traces the unit circle, figure 4.6(b). The resistance value at any point along this circle equals zero as the reactance changes from negative to positive infinity. The boundary points on the rectangular impedance plane where the vertical line extends to $\pm j$ infinity are transformed to the single point of (+1, 0). Similarly, the vertical line on the rectangular complex impedance plane that intersects a resistance value equal to infinity on the real axis is the smallest circle on the Smith chart with a radius of zero at the point (+1, 0). This example can be easily checked by inserting the appropriate values into Eq. (17). All resistance values from zero to infinity are represented on the Smith chart by circles, decreasing in diameter as their resistance value increases, figure 4.6(b). Because all constant-resistance contours are centered on the same axis and share a single common point of intersection, they are tangential to one another at this intersection point, (+1, 0).

4.5.3 Comparison of Tangential Contours

The τCAIC(90) and the Smith chart can be completely filled by their respective tangential circles (τCAICs and constant-resistance contours) in the complex plane. Both families of circles are centered on the real axis and both have only a single point, common to one another that represent an infinite-to-one transformation, a singularity point. The Smith chart is normalized and bounded by the unit circle because of the passive impedance reflection ($\Gamma \leq 1$) properties. The τ plane is not a normalized plane but is bound on the upper limit by the τCAIC(90). The Smith chart constant-resistance contours are centered on the real axis because they are normalized to a lossless characteristic impedance Z_0. Lossless is the common factor. The τCAICs are also centered on the real axis because the film and

substrate indices are lossless, that is completely real with no imaginary part.

The Smith chart is centered on the complex plane. It can be divided into half-circles either the real or the imaginary axis. Conversely, τCAICs never intersect the imaginary axis.

4.6 CONSTANT-THICKNESS and CONSTANT-REACTANCE CONTOURS

4.6.1 τ Plane Constant-Thickness Contours: Introduction

Horizontal lines of constant thickness on the $\phi_0 - d_r$ plane are successively transformed to constant-thickness contours in the X plane (XCTCs) and then to constant-thickness contours in the τ plane (τCTCs). Each τCTC is classified to a subfamily by its corresponding XCTC's intersection with the X plane real axis, see section 2.3.3. [1, 22]

Each τCTC starts on the τ plane real axis at the point (+1, 0) when $\phi_0 = 0°$. By holding the film thickness *d* constant and increasing the angle of incidence from 0 to 90°, each τCTC is projected into the τ plane as defined by its subfamily and ends at the corresponding point on the τCAIC(90). The four subfamilies are:

- SF1 = $\left\{ d : 0 < d \le \frac{D_{0^\circ}}{2} \right\} = \left(0,\ D_{0^\circ} \right]$
- SF2 = $\left\{ d : \frac{D_{0^\circ}}{2} < d < \frac{D_{90^\circ}}{2} \right\} = \left(\frac{D_{0^\circ}}{2},\ \frac{D_{90^\circ}}{2} \right)$
- SF3 = $\left\{ d : \frac{D_{90^\circ}}{2} \le d \le D_{0^\circ} \right\} = \left[\frac{D_{90^\circ}}{2},\ D_{0^\circ} \right]$
- SF4 = $\left\{ d : D_{0^\circ} < d \le D_{90^\circ} \right\} = \left(D_{0^\circ},\ D_{90^\circ} \right]$

A unique case to note is the zero thickness contour (ZTC). [29] This ZTC traces the real axis, beginning at (+1, 0), and extends positively with the increase in ϕ_0 until it reaches the point $\tau = N_1^2/N_0$ at $\phi_0 = 90°$.

4.6.1.1 τ Plane Constant-Thickness Contours: Subfamily 1

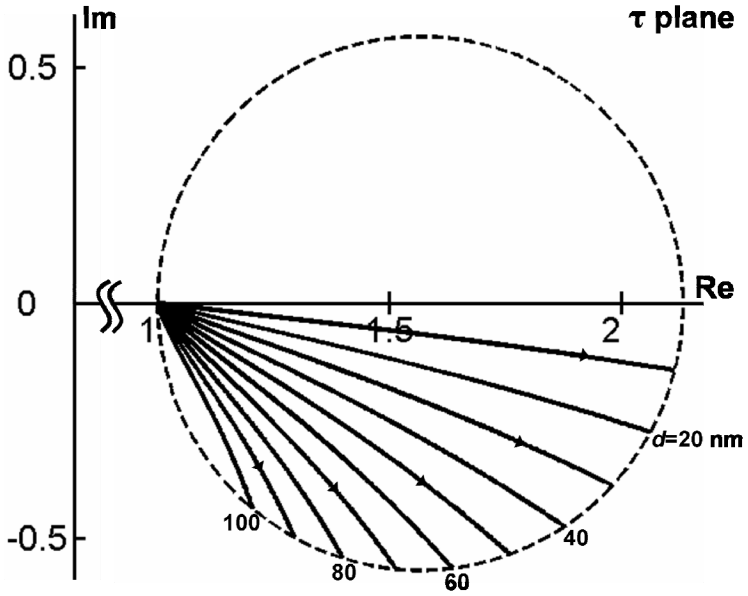

Figure 4.7: Subfamily 1 τCTCs for a zero film-substrate system where N_1 (N_2) = 1.46 (2.1316) at λ=632.8 nm. (A portion of the real axis has been intentionally removed to increase clarity.)

The first τCTC subfamily, SF1, comes from the $\phi_0 - d_r$ plane whose film thickness range is $0 < d \leq D_{0°}/2$. τCTCs in this thickness range are transformed into arcs on the X plane as XCTCs that do not intersect the real axis and are in the negative imaginary half plane, figure 2.5. With the second transformation of the TEF, the SF1 τCTCs are moved to the τ plane and are stacked clockwise, below the real axis, as the film thickness is increased. They begin at the point (+1, 0) where $\phi_0 = 0°$ and terminate on the τCAIC(90). Figure 4.7 illustrates the SF1 τCTCs for a zero film-substrate system where N_1 (N_2) = 1.46 (2.1316) at λ=632.8 nm. Each τCTC from figure 4.7 is relatively flat with little curvature.

4.6.1.2 τ Plane Constant-Thickness Contours: Subfamily 2

Horizontal lines on the $\phi_0 - d_r$ plane within the range of film thickness $D_{0^\circ}/2 < d < D_{90^\circ}/2$ are transformed to arcs on the X plane as XCTCs. [1] These XCTCs are classified as SF2 because they intersect the X plane real axis at the point (-1, 0), figure 2.5. SF2 XCTCs are subsequently transformed to the τ plane such that each contour not only begins at the point (+1, 0) but passes through it a second time before they terminate on the τCAIC(90). This X plane intersection with the negative real axis and τ plane intersection at (+1, 0) takes place when $(\phi_0, d) = (\phi_0, mD_{\phi 0}/2)$ on the $\phi_0 - d$ plane; figure 2.3.

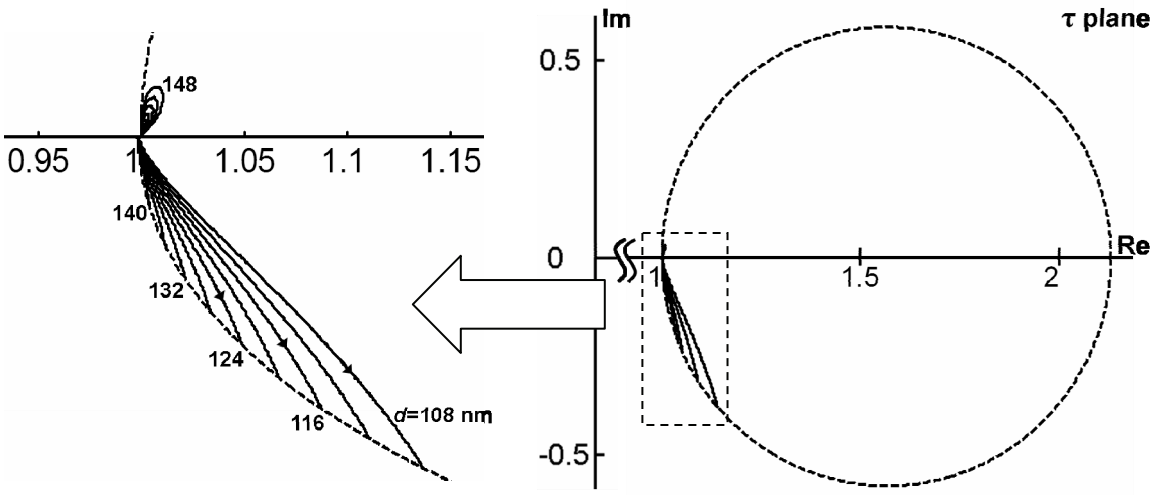

Figure 4.8: Subfamily 2 τCTCs for a zero film-substrate system where N_1 (N_2) = 1.46(2.1316) at λ=632.8 nm. SF2 exists in both the positive and negative imaginary half plane. It intersects the real axis when $d = D_{\phi 0}/2$. (A portion of the real axis has been intentionally removed to increase clarity.)

Subfamily 2 τCTCs begin by moving away from the (+1, 0) point with a positive slope and loop back counterclockwise to its point of origin (+1, 0), figure 4.8. They continues downward, adjacent to, but not overlapping with the last τCTC from SF1, terminating on its corresponding point on the τCAIC(90).

The SF2 τCTCs intersection with the τ plane real axis is derived from the successive transformation of $\phi_0 - d_r$ plane horizontal lines of constant-thickness to the τ plane. To clarify, a SF2 CTC (X and τ) has 3 parts associated with it: positive imaginary, real, and negative imaginary. If the ordered pair is $(\phi_0, d_r) = (\phi_0, d > D_{\phi 0}/2)$, then the point will be in the positive imaginary (X and τ) plane. When the ordered pair is $(\phi_0, d_r) = (\phi_0, d = D_{\phi 0}/2)$, it lies on the real axis of both planes. Finally, if the ordered pair is $(\phi_0, d_r) = (\phi_0, d < D_{\phi 0}/2)$, the point lies in the negative imaginary (X and τ) plane. All SF2 XCTCs start in the positive imaginary half plane, from an ordered pair above the $D_{\phi 0}/2$ curve on the $\phi_0 - d_r$ plane. This translates into an initially positive imaginary τCTC. As the XCTC grows larger with increased angle of incidence, it travels counter clockwise until it reaches the X plane real axis at (-1, 0), an ordered pair on the $D_{\phi 0}/2$ curve. Any ordered pair on the $D_{\phi 0}/2$ curve is transformed in an infinite-to-one transformation to the point (+1, 0) on the τ plane. Therefore, the SF2 τCTC must loop back and intersect through this point. When the XCTC arc passes through the real axis, the $\phi_0 - d_r$ plane ordered pair is below $D_{\phi 0}/2$ curve where it is then negative imaginary half plane (X and τ).

Notice in figure 4.8 that for a zero film-substrate system where N_1 (N_2) = 1.46 (2.1316) and λ=632.8 nm, SF2 only accounts for a small percentage of the entire τCAIC(90) domain. This figure illustrates the resulting transformation of the $D_{\phi 0}/2$ curve in the $\phi_0 - d_r$ plane to the τ plane, see figure 4.5(a).

4.6.1.3 τ Plane Constant-Thickness Contours: Subfamily 3

Subfamily 3 τCTCs are very similar to SF1 τCTCs, in that SF3 is also completely in an imaginary half plane, the positive. Horizontal lines on the $\phi_0 - d_r$ plane within the range of

film thickness $D_{90°}/2 \leq d \leq D_{0°}$ are transformed to the X plane as XCTCs. [1] These XCTCs are classified as SF3 because they do not intersect the X plane real axis and reside in the positive imaginary half plane, figure 2.5. The TEF transforms these arcs to τ plane constant-thickness contours in the positive imaginary half plane that do not intersect the real axis.

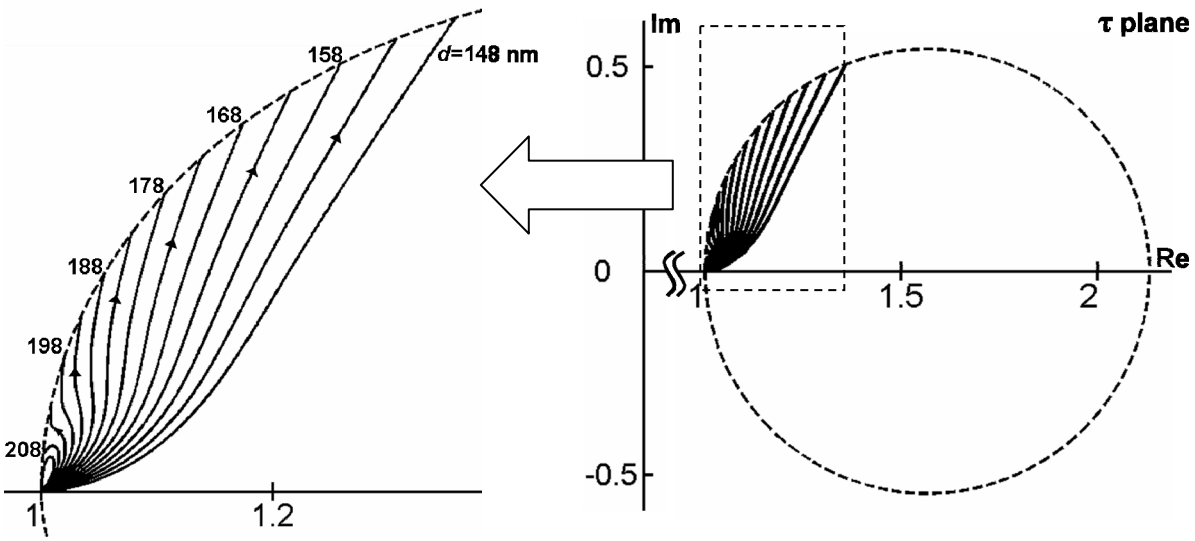

Figure 4.9: Subfamily 3 τCTCs for a zero film-substrate system where N_1 (N_2) = 1.46 (2.1316) at λ=632.8 nm. These SF3 τCTCs exist wholly in the positive imaginary half plane. (A portion of the real axis has been intentionally removed to increase clarity.)

From the zoomed view in figure 4.9, the τCTCs associated with lower film thicknesses in SF3 trace a counterclockwise contour, much like the positive imaginary portion of the SF2 τCTCs. They begin at the common origin point (+1, 0), travel up into the positive τ plane, loop back counterclockwise, and terminate near their point of origin. As the film thickness is increased, the resulting SF3 τCTCs terminate further and further away from the real axis.

4.6.1.4 τ Plane Constant-Thickness Contours: Subfamily 4

Subfamily 4 is composed of the horizontal lines of constant film thickness from the $\phi_0 - d_r$ plane that range from $D_{0^\circ} < d \leq D_{90^\circ}$. When these horizontal lines are transformed by Eq. (6) to the X plane as XCTCs each contour intersects the real axis at the point (+1, 0). It is this intersection with the positive X plane axis that classifies them as SF4.

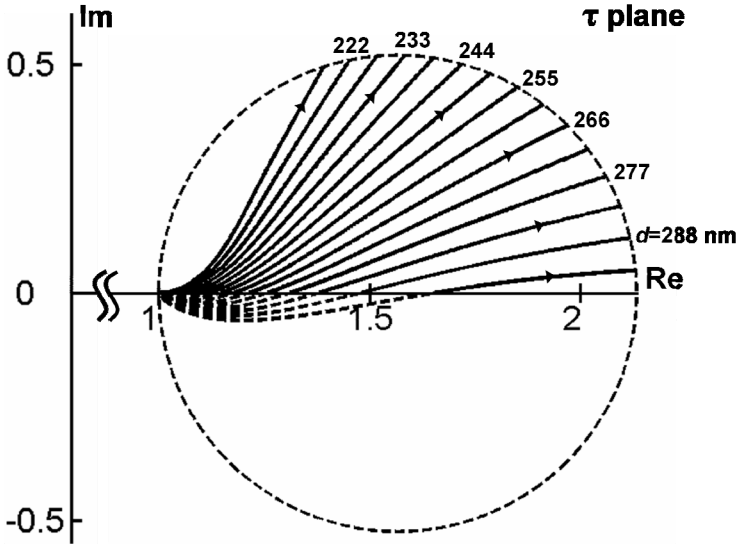

Figure 4.10: Subfamily 4 τCTCs for zero film substrate system where N_1 (N_2) = 1.46 (2.1316) at λ=632.8 nm. The dashed partial lines in the negative imaginary plane represent the horizontal part of constant thickness that is above the D_{ϕ_0} curve on the $\phi_0 - d_r$ plane. (A portion of the real axis has been intentionally removed to increase clarity.)

The portion of the XCTC that lies in the positive imaginary X plane is transformed to the positive imaginary half of the τ plane. The portion that lies in the negative imaginary X plane is transformed as an image in the negative τ half plane. Unlike the other three subfamilies where a horizontal line of constant thickness on the $\phi_0 - d_r$ plane spans 0° to 90°, the span of the SF4 lines of constant thickness are reduced to begin on the D_{ϕ_0} curve itself and end at 90°, see section 2.4.2 and figure 2.10. This is a result of the reduced

thickness plane, d_r, as explained in section 2.2. The section of the horizontal line from 0° to the $D_{\phi 0}$ curve within the SF4 thickness range is not actually in SF4. It lies above the $\phi_0 - d_r$ plane and is an image projected onto the $\phi_0 - d_r$ plane that overlaps SF1. [1, 22, 29] This image is presented as a dashed line on figure 4.10, see section 2.4.2.

4.6.2 Smith Chart Constant-Reactance Contours

Lines of constant reactance, horizontal lines on the rectangular complex impedance plane, figure 4.5(b), are transformed to the Smith chart as constant-reactance contours. These contours are arcs of circles that are tangents to the real axis at the point (+1, 0), figure 3.4. The contours are bound within the unit circle. The real axis of the rectangular complex impedance plane where the value of reactance equals zero is transformed to the real axis of the Smith chart as an arc of infinite radius. Positive imaginary reactances are transformed onto the Smith chart as inductive reactance contours in the positive imaginary half plane and negative imaginary reactances are transformed onto the Smith chart as capacitive reactance contours in the negative imaginary half plane, see figure 3.4. As the value of the reactance is increased, either positive or negative, the radii of these reactance contours are decreased. When the reactance is increased to either positive or negative infinity the arcs have radii of zero, and are transformed to the single point (+1, 0), figure 4.11(a).

Constant-reactance contours (arcs), both positive and negative are symmetric about the real axis as well. For example, an inductance contour has the same length and radius as the capacitive reactance contour of equal and opposite magnitude. This complex conjugate

relationship is carried over from the transformation of the rectangular impedance plane which is also symmetric about the real axis..

4.6.3 Comparison of Constant-Reactance and τ Plane Constant-Thickness Contours

By comparison, Smith constant-reactance contours and τCTCs have some obvious similarities. Both types of curves are derived from horizontal lines in their planes of origin and transformed by a bilinear equation. Both have families of curves that reside completely in the positive or negative imaginary half plane; figure 4.11 (a) and (b). Both types of curves share a single common point on the real axis (+1, 0) that represents an infinite-to-one transformation. And, both types of curves extend out of the point (+1, 0) and terminate on a circle that bounds its domain.

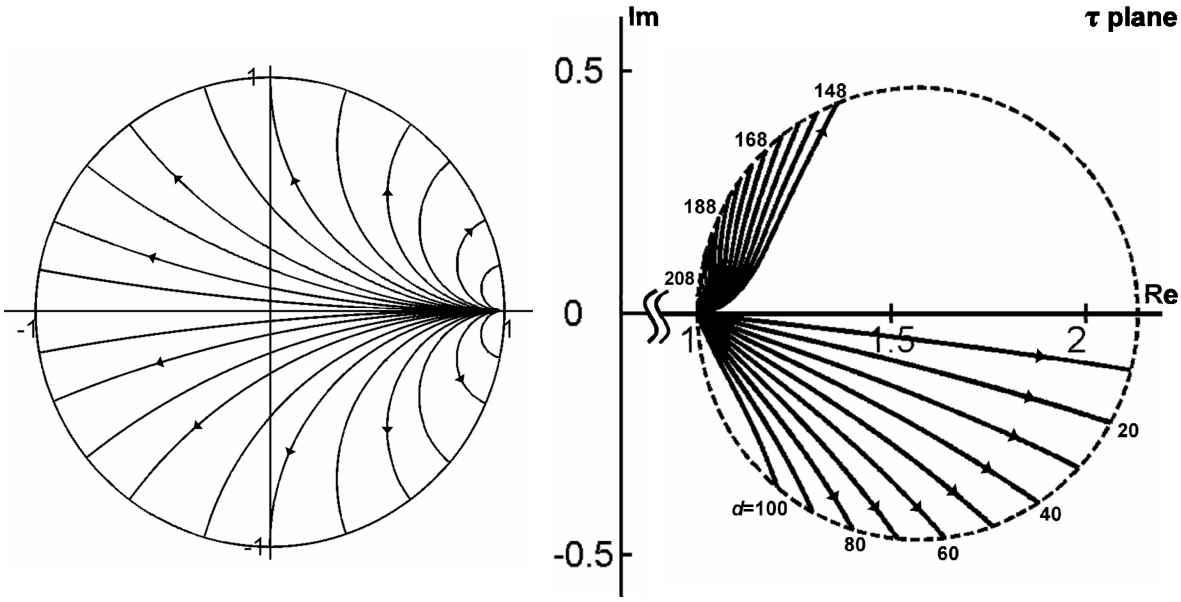

(a) (b)

Figure 4.11: (a) Smith chart constant-reactance contours and (b) τ plane SF1 and SF3 τCTCs for zero film-substrate system where N_1 (N_2) = 1.46 (2.1316) and λ=632.8 nm. SF1 is in the negative imaginary half plane and SF3 is in the positive imaginary half plane. (A portion of the real axis has been intentionally removed to increase clarity.)

This is where the similarities end. Whereas the capacitive and inductive reactance contours fill the domain of the Smith chart, the same cannot be said for the τ plane's SF1 and SF3 τCTCs even though they are also imaginary half plane subfamilies; figure 4.11(b) where capacitive contours correspond to SF1 and inductive contours correspond to SF3. This difference stems from their respective planes of origin. From section 4.3, the rectangular impedance plane, figure 4.5(b), is a uniform complex plane that encompasses both positive and negative imaginary half planes bisected by the real axis. Lines of constant reactance are parallel to the real axis as well as parallel to the plane boundaries at $\pm j\infty$. After its transformation to the Smith chart, this symmetric behavior still exists and the resulting reactance arcs are symmetric about the real axis allowing for complex conjugates.

The $\phi_0 - d_r$ plane is a non-uniform plane that is bisected by the $D_{\phi_0}/2$ curve. Lines of constant thickness are only parallel to the lower boundary of the plane where $d = 0$ nm. This results in SF1 τCTCs having less curvature and appearing flatter in comparison to SF2 and SF4 τCTCs. As the film thickness is increased, the τCTCs become more non-linear. This occurs because horizontal lines of constant thickness have a non-linear relationship to the $D_{\phi_0}/2$ (bisector) and D_{ϕ_0} curves (upper boundary).

The SF2 and SF4 τCTCs (SFs that intersect the real axis) do not exist on the Smith chart. Furthermore, a distinct advantage of the Smith chart is in its complex conjugates. This symmetry allows for a visual ease of use by being able to find impedance values in either the positive or negative imaginary half planes.

4.7 ORTHOGONALITY

The Smith chart is composed of two groups of contours (circles) whose centers lie on two axes that are perpendicular to each other. From elementary geometry, if two circles intersect whose centers lie on orthogonal axes, the intersections of the two circles occur at a perpendicular angle to each other. Therefore, every resistance and reactance curve on the Smith chart is orthogonal to each other.

The same is not true for τCTCs and τCAICs. Even though the τCAICs are non-intersecting circles whose centers lie on a common axis, the τCTCs are not circles, nor part of circles that share a common orthogonal axis. The only exception to this is the real axis. It represents a circle of infinite radius whose center lies on any perpendicular axis. Therefore, any intersection of τCAICs with the real axis occurs at orthogonal angles.

4.8 EFFECTS OF INCREASING MATERIAL INDICES

4.8.1 Introduction

The zero system has been defined by the specific relationship between the ambient, film, and substrate optical constants where $N_1 = \sqrt{N_0 \cdot N_2}$. Earlier in this chapter, a comparison was conducted on the contours of the zero film-substrate system where N_1 (N_2) = 1.46 (2.1316) at λ=632.8 nm and the Smith chart contours. Now, additional insight into the comparison using higher index materials is to be presented.

4.8.2 The $\phi_0 - d_r$ Plane

Although choosing a zero system whose material indices for film and substrate are

N_1 (N_2) = 3.0 (9.0) at λ=632.8 nm respectively, does not change any of the previous contour comparison analysis, it does result in flatter D_{ϕ_0} and $D_{\phi_0}/2$ curves on the $\phi_0 - d_r$ plane, figure 4.12. The range of film thickness spanned between the upper and lower limits of the $D_{\phi_0}/2$ curve of figure 4.5(a) is 13.569% of the total range of thickness spanned between the upper D_{90° limit and zero, since

$$\text{THICKNESS RANGE SPANNED (\%)} = \frac{\frac{D_{90^\circ}}{2} - \frac{D_{0^\circ}}{2}}{D_{90^\circ}} \text{ x } 100 \,. \qquad (20)$$

By increasing the index of the film to N_1 = 3.0, the percentage thickness range spanned between the upper and lower limits of the $D_{\phi_0}/2$ curve of its respective $\phi_0 - d_r$ plane, figure 4.12, is reduced to 2.859% and increasing N_1 to 5.0 further reduces the $D_{\phi_0}/2$ curve percentage thickness range to 1.01% in its respective $\phi_0 - d_r$ plane. Similarly, by replacing the appropriate $D_{\phi_0}/2$ curve limits with its respective D_{ϕ_0} curve limits in Eq. (20), the percentage thickness range spanned by the D_{ϕ_0} curve is reduced from 27.138% when N_1 = 1.46 to 5.718% when N_1 = 3.0, and to 2.02% when N_1 = 5.0.

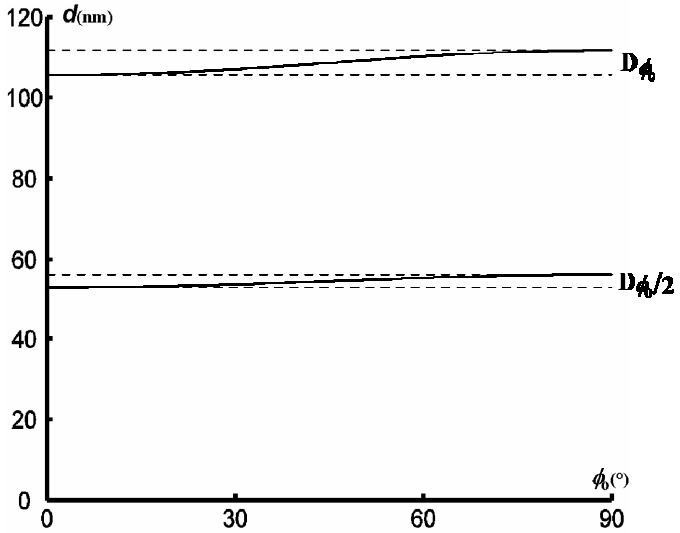

Figure 4.12: The $\phi_0 - d_r$ plane where N_0 = 1.0 and N_1 = 3.0 at λ=632.8 nm. The range of film thickness for SF2 and SF4 decrease as the film index is increased. As the range of film thickness for each curve is reduced, they are become flatter and more linear.

As the range of film thickness that spans the limits of the $D_{\phi 0}$ or $D_{\phi 0}/2$ curve in the ϕ_0 – d_r plane decreases with increased material indices, the overall $D_{\phi 0}$ or $D_{\phi 0}/2$ curve behavior flattens. When the film thickness range for $D_{\phi 0}$ or $D_{\phi 0}/2$ approaches its limit of a single thickness, the curve is a straight line. Consequently, the result of these relatively flatter $D_{\phi 0}$ or $D_{\phi 0}/2$ curves is a more linear transformation to the τ plane and a closer resemblance to the Smith chart.

4.8.3 τ Plane Constant-Angle-of-Incidence Contours (τCAICs)

Increasing the system indices does not change the general behavior of the τCAICs. The largest τCAIC occurs when $\phi_0 = 90°$ and all other τCAICs for the zero system are contained within it, intersecting tangentially at the point (+1, 0). As a reminder, the diameter of τCAIC(90) is a function of the film index: $N_1^2/N_0 - 1$. Therefore the τCAIC(90) is considerably large with higher film indices unless it is normalized by some parameter.

4.8.4 τ Plane Constant-Thickness Contours (τCTCs)

4.8.4.1 τ Plane Constant-Thickness Contours: Subfamily 1

As seen in figure 4.13, τCTCs in SF1 remain in the negative imaginary half plane when the material indices are increased. However, the τCTCs of the higher index system encompasses a larger percentage of its respective τCAIC(90). The τCTCs of higher index also have a noticeably larger curvature than those in the lower index system. The increased

curvature of the τCTCs has a closer resemblance to the Smith chart constant-reactance contours.

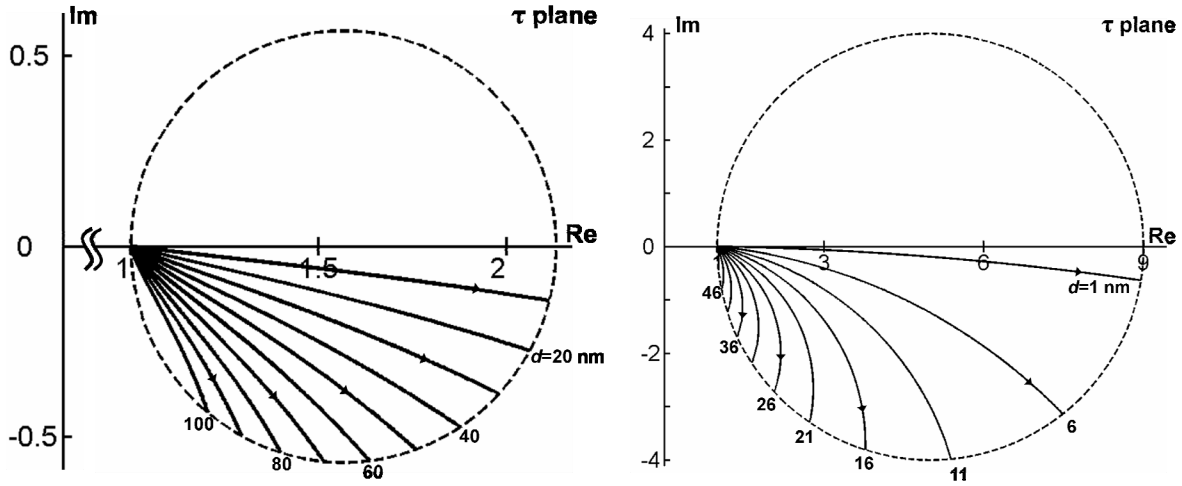

(a) (b)

Figure 4.13: Subfamily 1 τCTCs for N_1 (N_2) of (a) 1.46 (2.1316) and (b) of 3.0 (9.0) at λ=632.8 nm. The τCTCs for the system of higher material indices (b) fill a larger fraction of the τCAIC(90) than those τCTCs of the same subfamily of lower material indices.

4.8.4.2 τ Plane Constant-Thickness Contours: Subfamily 2

Increasing the film-substrate system indices results in a reduced range of thicknesses in subfamily 2. This is a direct result of a flatter $D_{\phi_0}/2$ curve on the $\phi_0 - d_r$ plane.

As the overall range of film thickness for $D_{\phi_0}/2$ is decreased, it contains fewer ordered pairs in its $\phi_0 - d_r$ plane domain. After transformation to the τ plane, the result is a reduced area of the τCTCs of SF2 in the domain of the τCAIC(90).

Figure 4.14clearly shows how the τCTCs of SF2 are closing in on the point (+1, 0) in the τCAIC(90) domain. When the $D_{\phi_0}/2$ curve is reduced to a single film thickness, it will lie on the real axis at the point (+1, 0) for any angle $(\phi_0, d_r) = (\phi_0, d = D_{\phi_0}/2)$, see section 4.6.1.2, an infinite-to-one transformation. Under this condition, the $\phi_0 - d_r$ plane bisector

will closely resemble the rectangular complex impedance plane bisector and the zero film-substrate system will closely resemble the Smith chart.

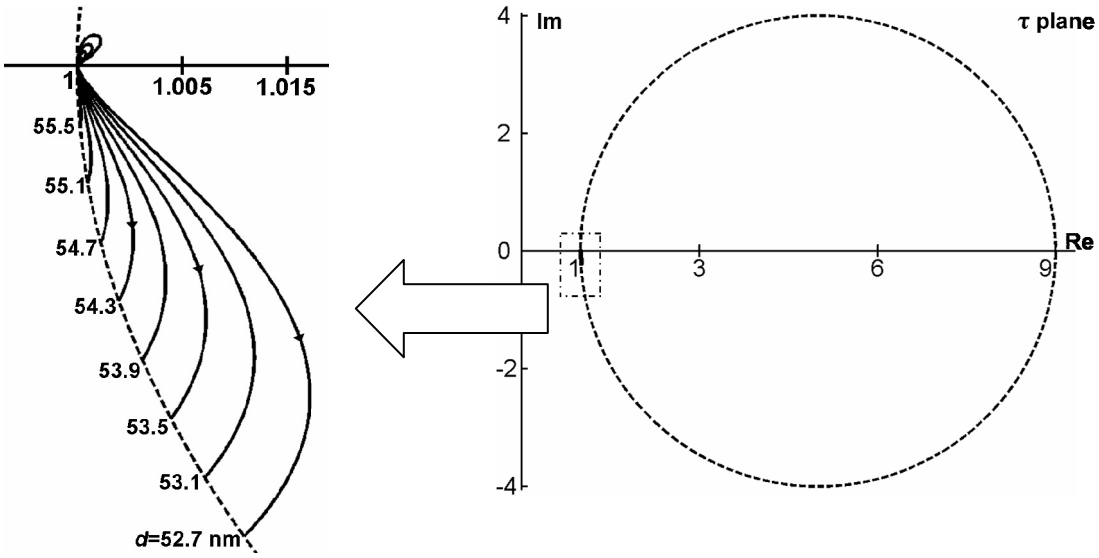

Figure 4.14: Subfamily 2 τCTCs for zero system whose N_1 (N_2) = 3.0 (9.0) at λ=632.8 nm. The area of the plane where SF2 exists is significantly smaller than the SF2 in figure 4.8 where N_1 (N_2) = 1.46 (2.1316) at λ=632.8 nm.

4.8.4.3 τ Plane Constant-Thickness Contours: Subfamily 3

Subfamily 3 τCTCs of higher material indices reside completely in the positive imaginary half plane, similar to those of lower material indices. In figure 4.15(b), the SF3 τCTCs of higher refractive indices cover a larger fraction of its respective τCAIC(90) area than the τCAIC(90) of lower refractive indices, figure 4.15(a). Similar to the higher index contours of SF1 in figure 4.13(b), the SF3 τCTCs have also become more arc-like in behavior resembling the Smith chart more than lower indices τCTCs.

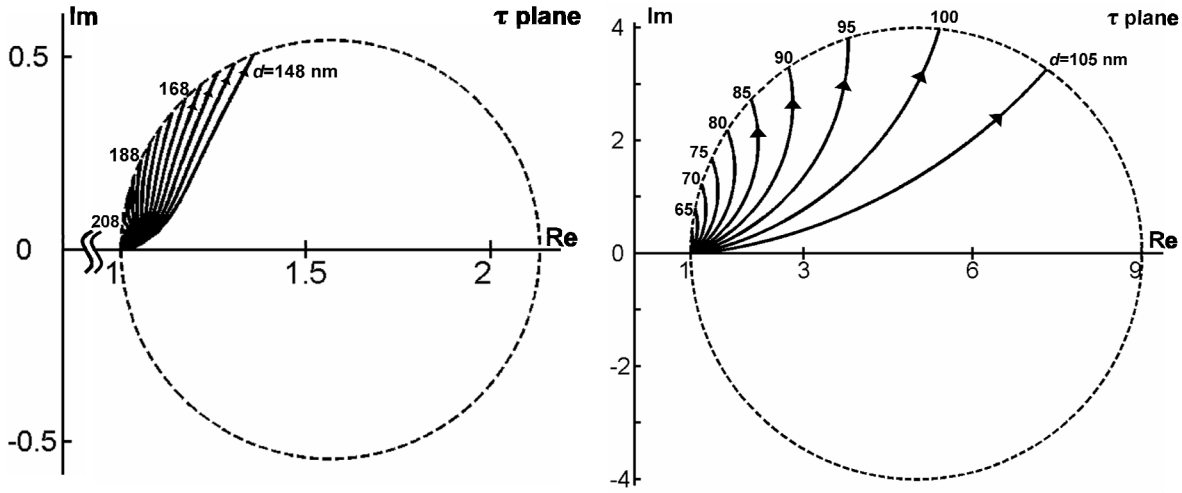

Figure 4.15: Subfamily 3 τCTCs for (a) N_1 (N_2) = 1.46 (2.1316) and (b) N_1 (N_2) = 3.0 (9.0) at λ=632.8 nm. The τCTCs for the system of higher material indices fill a larger fraction of the τCAIC(90) than those τCTCs from the same subfamily of lower material indices.

4.8.4.4 τ Plane Constant-Thickness Contours: Subfamily 4

Increasing the film-substrate indices also decreases the overall fraction of the τCAIC(90) area that is covered by the SF4 τCTCs. This is apparent in figures 4.16 where SF4 for the N_1 (N_2) = 1.46 (2.1316) system is compared next to the 3.0(9.0) film-substrate system. The SF4 area within its respective τCAIC(90) continues to decrease as the material indices are increased. Eventually, when the system indices are increased enough, the D_{ϕ_0} curve (SF4) on the $\phi_0 - d_r$ plane reduces to a single thickness, a straight line similar to the upper limit for the Smith chart. It is then transformed into the real axis on the τ plane.

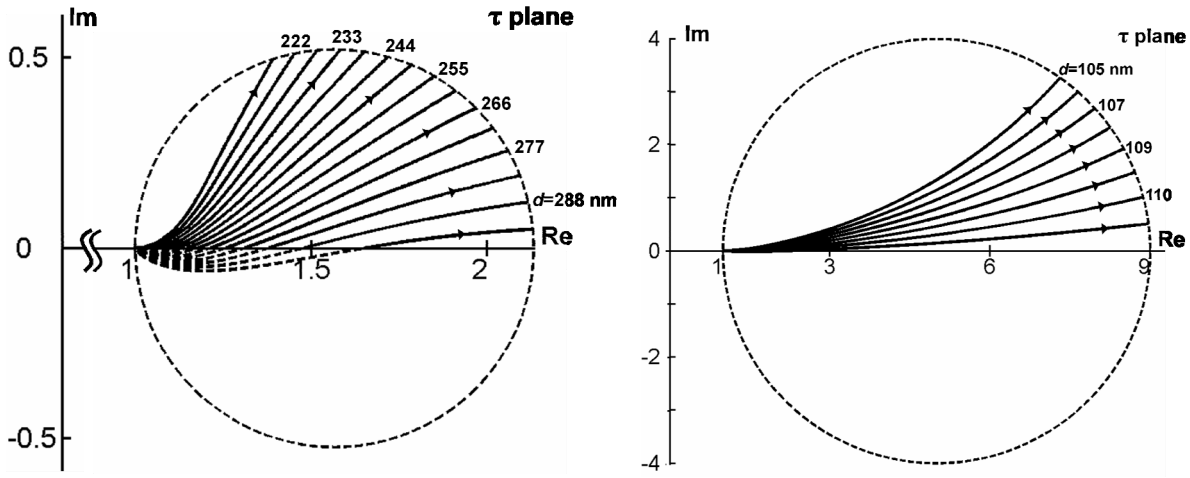

(a) (b)

Figure 4.16: Subfamily 4 τCTCs for (a) N_1 (N_2) = 1.46 (2.1316) and (b) N_1 (N_2) = 3.0 (9.0) at λ=632.8 nm. The dashed lines in the negative imaginary half plane represent an image of SF4 projected into the range of SF1. Figure (b) also has this image though it is not readily apparent from this view.

4.8.5 Subfamilies 1 and 3 Together

Figures 4.17 compare the SF1 and SF3 of a specific film-substrate system to the SF1 and SF3 of a film-substrate system of higher material indices. It is readily apparent that the τCTCs from the higher indices system fill up a significantly larger fraction of its respective τCAIC(90) than the τCTCs of the lower indices system.

Figure 4.18 shows SF1 and SF3 τCTCs of a zero film-substrate system where N_1=5.0 and N_2=25.0 at λ=632.8 nm. When compared to figures 4.17, the fractional area of the τCAIC(90) is near completely filled by the two imaginary half plane subfamilies. The individual τCTCs are becoming more circular in shape. The contours of SF1 and SF3 are becoming more symmetric and have an increased resemblance to the Smith chart than the film-substrate systems previously illustrated in figures 4.17.

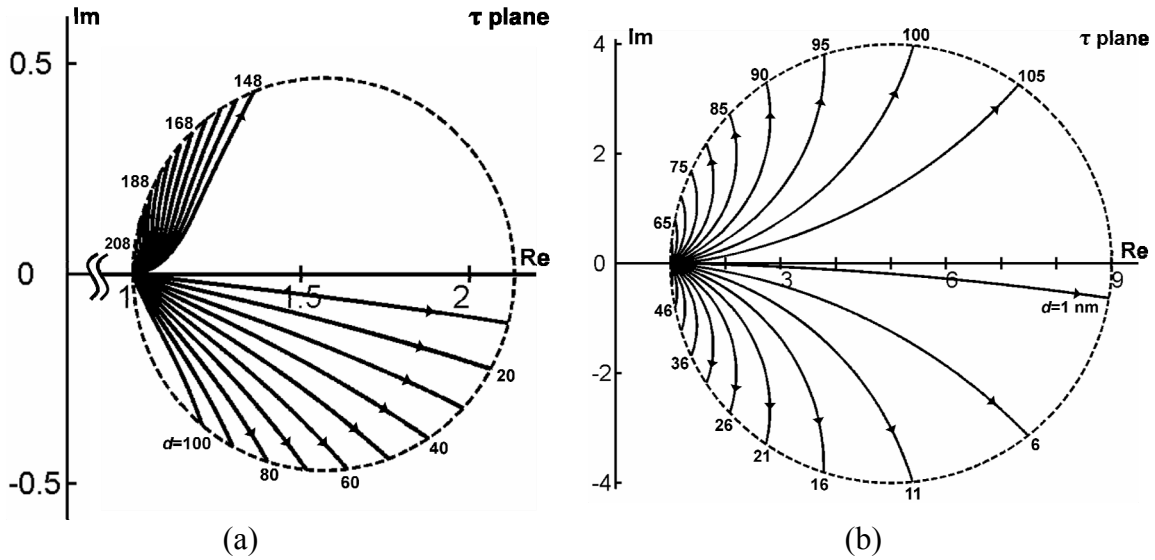

Figure 4.17: SF1 and SF3 τCTCs for (a) N_1 (N_2) = 1.46(2.1316) and (b) 3.0(9.0) at λ=632.8 nm. Imaginary half plane SF's (1 and 3) covering a larger fractional area of its respective τCAIC(90) as the film-substrate system indices are increased.

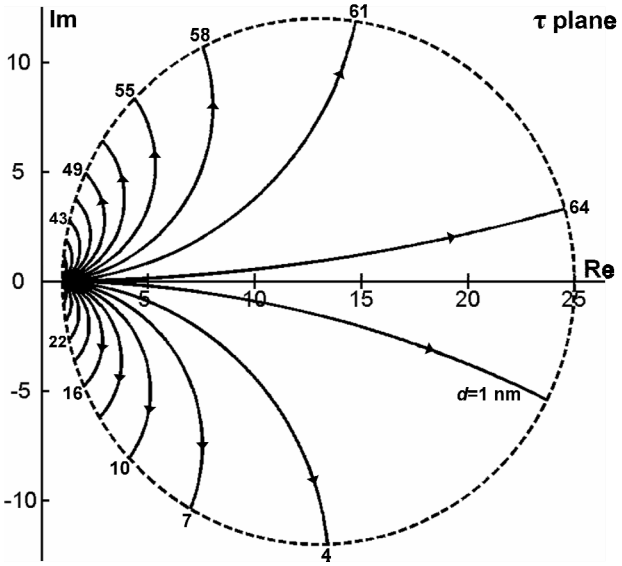

Figure 4.18: SF1 and SF3 where N_1 (N_2) = 5.0 (25.0) at λ=632.8 nm. Almost the entire plane is covered by these 2 imaginary half plane subfamilies.

CHAPTER V
CONCLUSIONS

A comparison of the constant-angle-of-incidence contours and constant-thickness contours of the transmission ellipsometric function (TEF) for a zero film-substrate system and the Smith chart contours has been presented. It was shown that both TEF and Smith chart have similar contours in both the positive and negative imaginary half planes. The Smith chart's contours originate from a complex plane with linear boundaries. It is bisected into symmetric positive and negative imaginary half planes of equal areas that are conjugate of each other. . When transformed to the Smith chart, it is normalized and the conjugate relationship remains intact. All contours in the positive imaginary half plane of the Smith chart are symmetric to all of the contours in the negative half plane of the Smith chart. TEF contours originate from a non-complex reduced thickness plane. This plane has a non-linear upper boundary. It is bisected into two equal areas but non-symmetric, half planes. When transformed to the complex τ plane, the likeness of the constant-angle-of-incidence contours and constant-thickness contours to the Smith chart contours become a function of the material indices. As the film-substrate system's material indices are increased, the range of the non-linear boundary of the $\phi_0 - d_r$ plane is reduced and the TEF contours more closely resemble the Smith chart. [30]

APPENDIX A

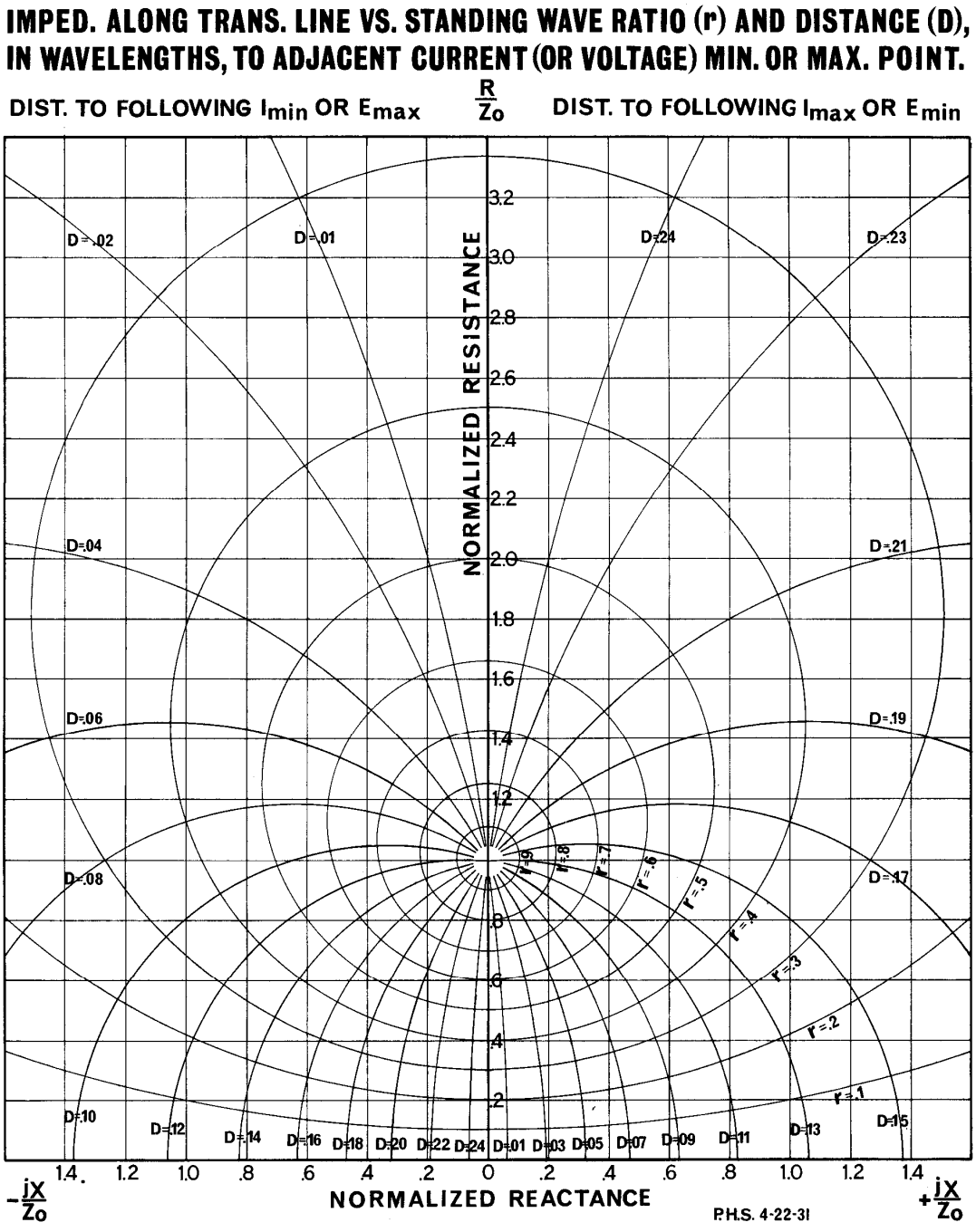

Figure A.1: Philip Smith's 1931 rectangular impedance chart. He later rotated it 90° clockwise so that the resistance axis would coincide with the real axis. [11]

REFERENCES

[1] A. R. M. Zaghloul, M. Elshazly-Zaghloul, W. A. Berzett, and D. A. Keeling, "Thin film coatings: An ellipsometric function approach I. Non-negative transmission systems, polarization-devices, coatings, and closed-form design formulae," submitted to Applied Optics (2006).

[2] R. M. A. Azzam and N. M. Bashara, *Ellipsometry and Polarized Light*, North-Holland, Amsterdam, 1977.

[3] R. M. A. Azzam, "Polar curves for transmission ellipsometry," Optical Communications, **14**, 145-147 (1975).

[4] P. Drude, "Uber Oberflaechenschichten. I. Theil," Annalen der Physik Und Chemie, **36**, 532-560 (1889).

[5] P. Drude, "Uber Oberflaechenschichten. II. Theil," Annalen der Physik Und Chemie, **36**, 865-8970 (1889).

[6] R. Jansson, H. Arwin, and I. Lundström, "Quasi three-dimensional, n-bit optical memory based on the ellipsometric principle: model calculations," Applied Optics, **33**, 6843–6854 (1994).

[7] R. Jansson, R. Wigren, K. Jarrendahl, I. Lundström, and H. Arwin, "A quasi three-dimensional optical memory with n-bit memory cells based on the ellipsometric principle: concept and prototype devices," Optical Communications, **104**, 277–279 (1994).

[8] M. Tazawa, G. Zu, and P. Jin, "Transparent ellipsometric memory with thin film multilayer structures optical memory based on the ellipsometric principle," Applied Surface Science, **212**, 402-405 (2003).

[9] A. R. M. Zaghloul, W. A. Berzett, and D. A. Keeling. "Design of transmission linear partial polarizers using a negative film-substrate system," Proceedings of the SPIE – The International Society for Optical Engineering, **5870**, 58700N (2005).

[10] P. H. Smith, "Transmission Line Calculator," Electronics, **12**, 29 (1939).

[11] P. H. Smith, *Electronic and Applications of the Smith chart*, McGraw-Hill, 1969.

[12] E. Borie and B. Jödicke, "Rieke diagrams for gyrotrons", International Journal of Infrared and Millimeter Waves, **11**, 243-250 (1990).

[13] K. Suzuki, “Graphical calculation method using the Smith chart for analyzing the frequency response of pneumatic transmission line systems,” Journal of the Japan Hydraulics and Pneumatics Society, **28**, 122-128 (1997).

[14] J. Rosner, “The Smith chart and quantum mechanics,” American Journal of Physics, **61**, 4 (1993).

[15] A. Victor, “Chart analysis enhanced with Mathcad,” Applied Microwave & Wireless, **13**, 50-60 (2001).

[16] V. Badii and H. M. Oloomi, “Transmission line application MATLAB toolbox based on the graphical design methods of the Smith chart,” Computer Applications in Engineering Education, **6**, 23-30 (1998).

[17] S. Malisuwan and M. Charoenwattanaporn, “Modified Smith-chart representation as applied to microstrip antenna design for wireless LAN applications,” 2003 IEEE International Symposium on Electromagnetic Compatibility *(IEEE Cat. No.03EX666)*, **1**, 150-153 (2003).

[18] F. Sagnard, “Educational Graphical Interfaces to Learn About Radiation and Propagation of Electromagnetic Waves,” IEEE Transactions on Education, **47**, (2004).

[19] C. Peng, R. Liang, J. K. Erwin, W. Bletscher, K. Nagata, and M. Mansuripur, “Determination of optical constants of thin films and multilayer stacks by use of concurrent reflectance, transmittance, and ellipsometric measurements,” Applied Optics, **40**, (2001).

[20] This classification is introduced for the reflection ellipsometric function in reference [21]. It is also valid for TEF.

[21] M. S. A. Yousef and A. R. M. Zaghloul, “Ellipsometric function of a film-substrate system: characterization and detailed study,” Journal Optical Society of America A, **6**, 355-366 (1982).

[22] A. R. M. Zaghloul and M. S. A. Yousef, “Unified analysis and mathematical representation of film-thickness behavior of film-substrate systems,” Applied Optics, **45**, 235-264 (2006).

[23] American Radio Relay League, *The AARL antenna book*, Newington, Conn., 18th Ed, 1997.

[24] W. Hayt and J. Buck, *Engineering Electromagnetics*, 7th Ed, Mcgraw-Hill, New York, 2005.

[25] Only the right half of the complex impedance plane is transformed. A negative impedance requires an active device, which is not our case.

[26] H. A. Macleod, *Thin-Film Optical Filters*, Elsevier, New York, 1969.

[27] C. C. Franck and J. B. Franck, "Preliminary study of the admittance diagram as a useful tool in the design of stripline components at microwave frequencies," SPIE Current Developments in Optical Design and Optical Engineering, **1527**, 277-290 (1991).

[28] S. S. Bor *et al*, "Plots with matching circles for optimizing the performance of a low-noise amplifier," Microwave and Optical Technology Letters, **6**, 141-148 (1993).

[29] R. M. A. Azzam, A. R. M. Zaghloul, and N. M. Bashara, "Ellipsometric function of a film-substrate system: applications to the design of reflection-type optical devices and to ellipsometry," Journal Optical Society of America, **65**, 252-260 (1975).

[30] W. A. Berzett and A. R. M. Zaghloul, "The Transmission Ellipsometric Function contours and the Smith chart," Applied Optics (2006), in preparation.